Variations of Primary Productivity in the Northwestern Arabian Sea During the Last 23,000 Years and Their Paleoclimatological Implications

Xinquan Zhou, Stéphanie Duchamp-Alphonse, Masa Kageyama, Franck Bassinot, Florian Doressoundiram, Catherine Kissel

▶ **To cite this version:**

Xinquan Zhou, Stéphanie Duchamp-Alphonse, Masa Kageyama, Franck Bassinot, Florian Doressoundiram, et al.. Variations of Primary Productivity in the Northwestern Arabian Sea During the Last 23,000 Years and Their Paleoclimatological Implications. Paleoceanography and Paleoclimatology, 2022, 37 (10), pp.1306. 10.1029/2022PA004453 . hal-03874269

HAL Id: hal-03874269
https://hal.science/hal-03874269

Submitted on 28 Nov 2022

HAL is a multi-disciplinary open access archive for the deposit and dissemination of scientific research documents, whether they are published or not. The documents may come from teaching and research institutions in France or abroad, or from public or private research centers.

L'archive ouverte pluridisciplinaire **HAL**, est destinée au dépôt et à la diffusion de documents scientifiques de niveau recherche, publiés ou non, émanant des établissements d'enseignement et de recherche français ou étrangers, des laboratoires publics ou privés.

Distributed under a Creative Commons Attribution 4.0 International License

Check for updates

Paleoceanography and Paleoclimatology

AGU ADVANCING EARTH AND SPACE SCIENCE

RESEARCH ARTICLE
10.1029/2022PA004453

Variations of Primary Productivity in the Northwestern Arabian Sea During the Last 23,000 Years and Their Paleoclimatological Implications

Xinquan Zhou[1], Stéphanie Duchamp-Alphonse[1], Masa Kageyama[2], Franck Bassinot[2], Florian Doressoundiram[1,2], and Catherine Kissel[2]

[1]Université Paris-Saclay, CNRS, GEOPS, Orsay, France, [2]Laboratoire des Sciences du Climat et de l'Environnement, CEA/CNRS/UVSQ, Université Paris-Saclay, Centre CEA-Saclay, Gif-sur-Yvette, France

Key Points:

- Past primary productivity (PP) and upwelling in the NW Arabian Sea are reconstructed by coccolith assemblages from a marine sediment core
- PP was relatively high during the cold periods compared to the warm periods of the last 23 Kyr
- PP changes were mainly controlled by winter monsoon through changes in convective mixing and by aeolian inputs

Supporting Information:

Supporting Information may be found in the online version of this article.

Correspondence to:

X. Zhou,
xinquan_zhou@tongji.edu.cn

Citation:

Zhou, X., Duchamp-Alphonse, S., Kageyama, M., Bassinot, F., Doressoundiram, F., & Kissel, C. (2022). Variations of primary productivity in the northwestern Arabian Sea during the last 23,000 years and their paleoclimatological implications. *Paleoceanography and Paleoclimatology*, *37*, e2022PA004453. https://doi.org/10.1029/2022PA004453

Received 29 MAR 2022
Accepted 6 OCT 2022

Author Contributions:

Conceptualization: Xinquan Zhou, Stéphanie Duchamp-Alphonse
Data curation: Xinquan Zhou
Investigation: Xinquan Zhou, Florian Doressoundiram
Methodology: Xinquan Zhou, Masa Kageyama
Resources: Franck Bassinot, Catherine Kissel
Supervision: Stéphanie Duchamp-Alphonse, Masa Kageyama
Visualization: Xinquan Zhou

© 2022. The Authors.
This is an open access article under the terms of the Creative Commons Attribution License, which permits use, distribution and reproduction in any medium, provided the original work is properly cited.

Abstract The Arabian Sea (AS) is one of the most productive oceanic regions in the world due to several monsoon-related processes that can increase nutrients contents in the euphotic zone. Previous studies of the imprint of oceanic primary productivity (PP) in AS sediments yielded diverse results depending on the studied area and the chosen proxies, with unprecise paleoclimatic interpretations. Here, we provide multi-decennial PP and coastal upwelling dynamic records off northern Oman over the last 23 Kyr, based on the analysis of coccoliths from sediment core MD00-2354. Our results have been compared with previous paleoenvironmental records as well as new modeling data to get precise paleoclimatic interpretations. We document higher PP and weaker coastal upwelling during the Last Glacial Maximum relative to the Holocene, and significant millennial-scale variations over the last deglaciation corresponding to the fluctuations of the Atlantic Meridional Overturning Circulation strength. Higher PP and weaker upwelling are found during the cold stadials, while lower PP and stronger upwelling during the warm interstadial. We propose that the increases of PP were driven by increased bioavailable nutrient content in surface waters under both stronger winter monsoon conditions that strengthened the convective mixing, and higher aeolian inputs. Over the Holocene, stronger upwelling and slightly lower PP are found during the Early-Mid Holocene, when higher summer insolation triggered stronger summer monsoon. At that time, the lower PP was probably the result of restricted advection of eutrophic summer upwelling seawater under negative wind stress curls and less aeolian inputs.

Plain Language Summary Ocean primary productivity (PP) is the production rate of organic carbon from inorganic carbon by ocean phytoplankton through photosynthesis, in which nutrients and sunlight are necessary. In tropical oceans, this rate is usually limited by the availability of nutrients in the sunlit ocean, which is controlled by physical processes such as seawater upward motion, ocean mixing, and dust storms. All these processes play a significant role in the northwestern Arabian Sea (AS) today. It is surrounded by arid lands that provide the highest amount of airborne material in the world and it is influenced by the Indian monsoon system that drives seawater upward motion and mixing in summer and winter, respectively. However, not much is known about their impact on PP in the past. This work aims to reconstruct changes of PP in the northwestern AS over the past twenty thousand years and understand by which process(es) they are impacted, based on a model-data comparison approach. We have found that PP was higher during cold periods than during warm ones. The changes were mainly controlled by both, winter monsoon through changes in convective mixing, and dust storms through changes in nutrient-enrich aeolian inputs.

1. Introduction

The Arabian Sea (AS) is one of the most productive oceanic regions in the world due to the important supply of nutrients to the euphotic zone either from below, through wind-driven coastal upwelling or surface cooling-driven convective mixing, and/or from surrounding continents, through the transport and deposition of fertilizing aeolian dust (Bali et al., 2019; Jickells et al., 2005; Lee et al., 2000; Prasanna Kumar & Narvekar, 2005). This semi-enclosed basin is under the influence of the Indian monsoon system, characterized by seasonal shifts of prevailing surface winds and precipitations that shape the AS upper circulation and stratification and thus, nutrient and primary productivity (PP) distributions (Lévy et al., 2007; Schott & McCreary, 2001; Wang & Ding, 2008). During the summer monsoon that is, from May to September, faster heating of the Asian continent relative to the Indian Ocean creates a land-sea temperature (pressure) gradient that drives strong and wet

25724525, 2022, 10, Downloaded from https://agupubs.onlinelibrary.wiley.com/doi/10.1029/2022PA004453 by Cochrane France, Wiley Online Library on [27/11/2022]. See the Terms and Conditions (https://onlinelibrary.wiley.com/terms-and-conditions) on Wiley Online Library for rules of use; OA articles are governed by the applicable Creative Commons License

25724525, 2022, 10, Downloaded from https://agupubs.onlinelibrary.wiley.com/doi/10.1029/2022PA004453 by Cochrane France, Wiley Online Library on [27/11/2022]. See the Terms and Conditions (https://onlinelibrary.wiley.com/terms-and-conditions) on Wiley Online Library for rules of use; OA articles are governed by the applicable Creative Commons License

Writing – original draft: Stéphanie Duchamp-Alphonse
Writing – review & editing: Masa Kageyama, Franck Bassinot, Catherine Kissel

southwesterly winds running diagonally across the AS, which contribute to the development of a clockwise upper ocean circulation. Associated with intense alongshore winds and Ekman pumping, a strong coastal upwelling develops off Somalia and Oman that brings cold and nutrient-rich waters to the euphotic zone and helps sustaining a high PP cell extending up to the central part of the basin (Bartolacci & Luther, 1999; Lee et al., 2000; Prasanna Kumar, Madhupratap, et al., 2001; Figure 1). During the winter monsoon that is, from November to March, as the land-sea temperature (pressure) gradient is opposite due to faster land cooling relative to the Indian Ocean, dry and cold northeasterly winds blow from the Asian continent. They result in an anti-clockwise upper ocean circulation associated with a convective mixing north of 15°N that leads to the development of a high PP cell in the northern part of the AS as cold and nutrient-rich intermediate waters resurface (Schott & McCreary, 2001; Prasanna Kumar & Narvekar, 2005; Prasanna Kumar, Ramaiah, et al., 2001; Figure 1). The AS is also surrounded by vast (supra-) arid lands that provide the highest amount of airborne material in the world during dust storms (Francis et al., 2021; Mashat et al., 2018; Notaro et al., 2015; Ramaswamy et al., 2017; Rea, 1994; Rezazadeh et al., 2013; Yu et al., 2013). This material brings a combination of essential nutrients to the euphotic zone of the AS, such as nitrogen, phosphorus, and iron that contribute to maintain high PP through the year (Bali et al., 2019; Banerjee & Prasanna Kumar, 2014; Guieu et al., 2019; Jickells et al., 2005; Patra et al., 2007; Singh et al., 2008).

The imprint of PP in marine sediments from the AS has already been the focus of studies that aimed at understanding the interaction of the Indian monsoon and global climate. Numerous organic (total organic carbon [TOC], biomarkers) and inorganic (biogenic silica and barium, planktonic foraminifera) proxies have been measured in sediment cores from the western and northwestern AS in order to identify changes in the southwest summer monsoon (indicated by coastal upwelling dynamic) at glacial-interglacial (Anderson & Prell, 1993; Emeis et al., 1995; Reichart et al., 1997; Shimmield et al., 1990; Weedon and Shimmield, 1991; Ziegler et al., 2010) and tectonic (Bialik et al., 2020) time scales. Authors concluded about higher PP during interglacial periods compared to glacial ones due to stronger summer monsoon conditions as minimum ice volume in the Northern Hemisphere reduce snow cover over central Asia and increase the land-sea temperature (pressure) gradient. These results are consistent with the centennial to millennial PP changes recorded over the last deglaciation that show higher PP during the mild interstadial Bølling-Allerød (B-A; 14.7–12.9 ka), and lower PP during the near-glacial stadials Heinrich Stadial 1 (HS1; 17–14.7 ka) and Younger Dryas (YD; 12.9–11.7 ka), in reaction to rapid temperature fluctuations of high northern latitudes (Balaji et al., 2018; Caley et al., 2013; Deplazes et al., 2014; Gupta et al., 2013; Ivanochko et al., 2005; Schulz et al., 1998). Such fluctuations reflect the injection of melt water into the North Atlantic Ocean that regulates the strength of the Atlantic Meridional Overturning Circulation (AMOC), an important process that modulates the interhemispheric heat transport and thus, the intensity of the summer monsoon circulation (Kageyama, Merkel, et al., 2013; Marzin et al., 2013; McManus et al., 2004; Murton et al., 2010). However, these results differ from a few studies that testify for higher PP during glacial periods due to stronger winter monsoon and enhanced fertilization by aeolian input due to increased aridity on the adjacent continents (Pourmand et al., 2007; Tamburini et al., 2003). One could have hypothesis a regional difference between nearshore and offshore studied areas, the latter possibly experiencing further influence of winter monsoon conditions than the former ones. However, the aforementioned records do not follow this hypothesis, as the PP reconstruction from Tamburini et al. (2003) comes from the exact Oman margin. Another could have question the accuracy of the organic and inorganic proxies that have been used to infer PP as they additionally depend upon oxygenation and preservation conditions at the seafloor (especially TOC and biogenic barium) (e.g., Lückge et al., 1999), which make it difficult to disentangle PP variations from changes in bottom water conditions. However, even if these data are not representative of quantitative PP that is a signal restricted to the euphotic zone, they have been obtained based on multi-proxy approaches from several sites, associated with specific preservational conditions that, in no case, may lead to similar PP signals. Answer is more likely to be found in model-proxy modeling studies that include marine biogeochemical components. Bassinot et al. (2011) and Le Mézo et al. (2017) are the only ones to simulate PP patterns in response to changed boundary conditions in the past (e.g., Mid-Holocene [MH] and Last Glacial Maximum [LGM]) considering both summer and winter monsoons, based on the IPSL-CM4 and IPSL-CM5A-LR models. Particularly, Le Mézo et al. (2017) weakens the usual paradigm that a stronger summer monsoon should induce a stronger upwelling and thus increased PP in the AS, further highlighting the urge to compare modeling results to high-resolution PP reconstructions from sites under the influence of both, summer and winter monsoon conditions.

In this study, we provide the first millennial-scale records of paleo-PP and coastal upwelling dynamics in the northwestern AS over the last ∼23 Kyr, based on the analysis of coccolith assemblages from the sediment core

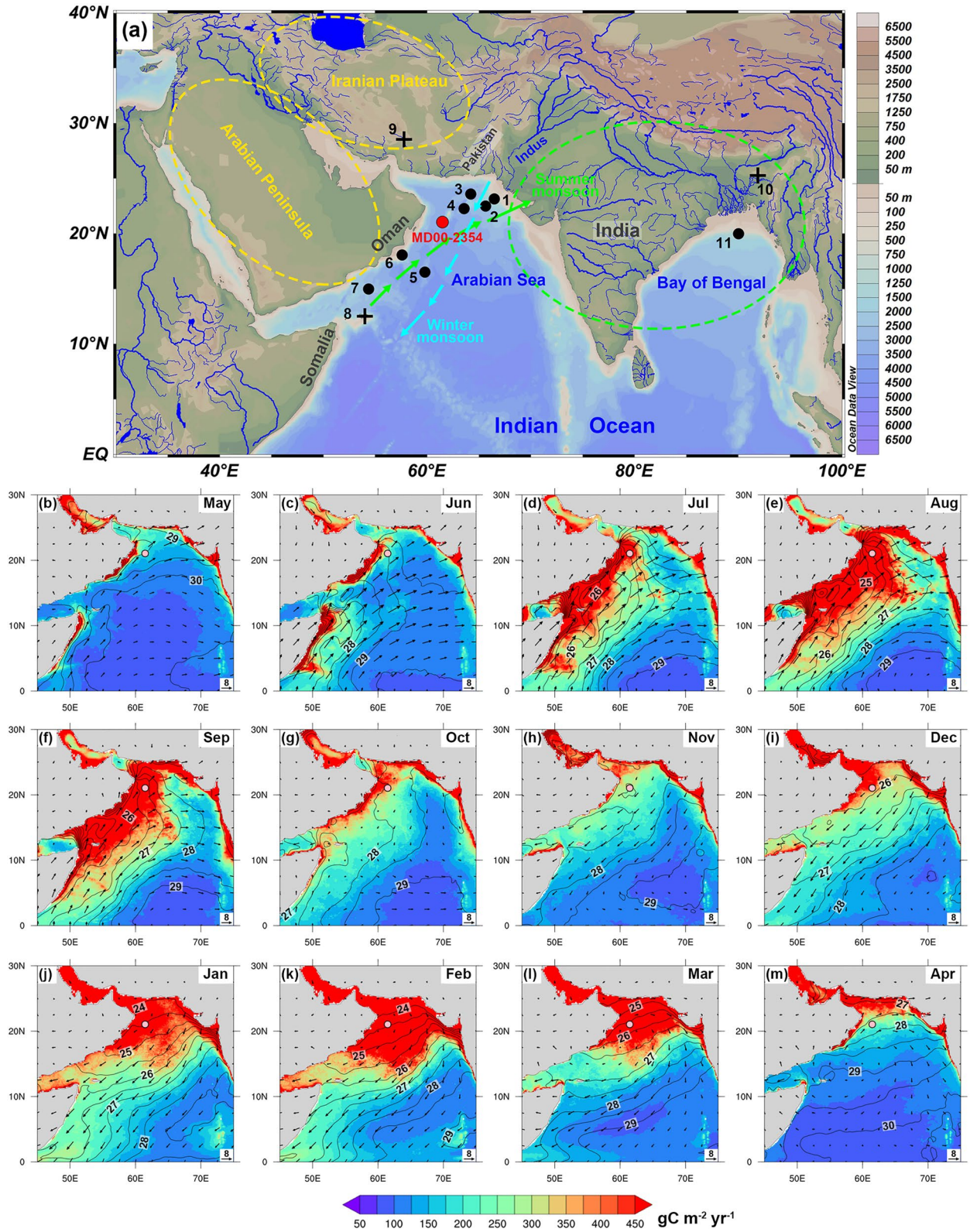

Figure 1.

25724525, 2022, 10, Downloaded from https://agupubs.onlinelibrary.wiley.com/doi/10.1029/2022PA004453 by Cochrane France, Wiley Online Library on [27/11/2022]. See the Terms and Conditions (https://onlinelibrary.wiley.com/terms-and-conditions) on Wiley Online Library for rules of use; OA articles are governed by the applicable Creative Commons License

25724525, 2022, 10, Downloaded from https://agupubs.onlinelibrary.wiley.com/doi/10.1029/2022PA004453 by Cochrane France, Wiley Online Library on [27/11/2022]. See the Terms and Conditions (https://onlinelibrary.wiley.com/terms-and-conditions) on Wiley Online Library for rules of use; OA articles are governed by the applicable Creative Commons License

MD00-2354 (61.48°E and 21.04°N). Surface waters at that site are under the influence of the coastal upwelling off Oman and the convective mixing cell off Iran/Pakistan that drive high PP during summer and winter, respectively (Figure 1), and receive important amount of airborne nutrients derived from dust storms in the Arabian Peninsula and Iranian Plateau (Kumar et al., 2020). Overall, they are far from the influence of main rivers that flow in the southeastern region of Pakistan (especially the Indus River) (Shimmield et al., 1990). The last ~23 Kyr encompasses a glacial-interglacial transition, an entire precessional cycle, and important fluctuations in the AMOC during the last deglaciation (McManus et al., 2004). It is therefore a perfect case study to explore the impact of key climate forcing mechanisms on PP for both, past and future climate conditions, such as ice sheet volume, sea level, and atmospheric CO_2 concentration. Coccoliths, which are the calcite scales produced by unicellular coccolithophore algae, are abundant in marine sediments, and have been used worldwide to infer physio-chemical conditions of the euphotic zone in the past. The species *Florisphaera profunda* in particular, that is restricted to the lower euphotic zone (water depths of 100–200 m), has been widely used to reconstruct variations in the nutricline depth (e.g., Bassinot et al., 1997; C. Liu et al., 2008; Molfino & McIntyre, 1990; Okada & Honjo, 1973; Okada & Mastsuoka, 1996; Su et al., 2013), and hence in PP (e.g., Beaufort et al., 1997; Beaufort et al., 2010; de Garidel-Thoron et al., 2001; Zhang et al., 2016; Zhou et al., 2020). The species *Calcidiscus leptoporus* that flourishes in mixed and nutrient-rich waters (Gravalosa et al., 2008; Ziveri et al., 1995), has been used for reflecting nutrient contents in coastal upwelling settings (Baumann et al., 2016; Boeckel et al., 2006; Fincham & Winter, 1989; Giraudeau, 1992; Giraudeau & Rogers, 1994; Saavedra-Pelitero et al., 2010). In the AS, highest fluxes of *C. leptoporus* were found in sediment traps off Somalia during summer coastal upwelling events (H. A. Andruleit et al., 2000; Broerse et al., 2000; Renaud et al., 2002), and it is most probable that this pattern remained so in the past. We combine our micropalaeontological data (*F. profunda*-based PP and *C. leptoporus* abundance) with previous records of direct and indirect PP (low-resolution *F. profunda*-based PP and TOC mass accumulation rates), upwelling dynamic (percentage of foraminifera *Globigerina bulloides*), sea surface temperature (SST; alkenones), and aeolian inputs (^{230}Th-normalized detrital flux and Ti_{XRF}) in the northern and northwestern AS. We also compare our reconstructed PP with outputs of the Earth System model IPSL-CM5A-LR (termed IPSL-CM5A in the following) and the transient simulation TraCE-21 (termed TraCE in the following). This allows us to evaluate the response of PP to changing surface oceanic and atmospheric conditions over the last ~23 Kyr, with a special focus on the LGM (21 ka) and the MH (6 ka).

2. Materials and Methods

2.1. Core Location and Age Model

Core MD00-2354 was collected in the northwestern AS, about 210 km off the Oman Margin, onboard the *R.V. Marion Dufresne*, in 2000. It is located on the southwestern slope of the Murray Ridge, at 2,740 m water depth that is, above the modern lysocline (~3,300 m; Cullen & Prell, 1984). Fossil coccolith records from this area have great potentials to successfully monitor and reconstruct paleoceanographic conditions (H. Andruleit & Rogalla, 2002; H. Andruleit et al., 2004). The lithology of this sediment core mainly consists of homogenous gray clay and foraminifera- and coccolith-bearing oozes. Its age model has been established by Böll et al. (2015) based on the correlation of the $\delta^{18}O$ signal obtained on foraminifera *Globigerinoides ruber* ($\delta^{18}O_{G.\ ruber}$) to the $\delta^{18}O_{G.\ ruber}$ record of 74KL sediment core retrieved in the western AS, in turn, correlated to the $\delta^{18}O$ signal of GISP2 ice core (Stuiver & Grootes, 2000). The upper 3 m of the sediments span the last 23.3 Kyr, with a sedimentation rate ranging between ~10 and 110 cm Kyr^{-1} (Figure S1 in Supporting Information S1).

Figure 1. (a) Geographic setting and bathymetric map created by the Ocean Data View software (©Reiner Schlitzer, Alfred Wegener Institute) with its built-in global high-resolution bathymetric data (GlobHR). The red dot marks the location of the studied core MD00-2354. The black dots and crosses mark the locations of cores with published micropaleontological and geochemical data that have been used in this study. Numbers 1 to 11 refer to site names as follow: 1 = 136KL; 2 = 94KL; 3 = 93KL; 4 = NIOP464; 5 = RC-27-42; 6 = ODP723A; 7 = GeoB 3005; 8 = Moomi Cave; 9 = Konor Sandal peat boot; 10 = Mawmluh Cave; 11 = 126KL. The green and blue arrows schematically depict the summer southwesterlies (Findlater Jet) and winter northeasterlies over the Arabian Sea (AS). The green dashed circle indicates the area of summer monsoon rainfall (Wang & Ding, 2008). The yellow dashed circle shows potential source areas of the aeolian dust transported to the AS (Sirocko et al., 1991, 2000). (b–m) Climatology (period 2003–2019) of PP (color, gC m^{-2} yr^{-1}), sea surface temperature (SST; contours, °C), and surface wind (vectors, m s^{-1}). PP was calculated by the standard VGPM model based on the MODIS chlorophyll-a concentration data set (Behrenfeld & Falkowski, 1997). PP data are from the "Ocean Productivity" website (http://sites.science.oregonstate.edu/ocean.productivity). SST data are from the NOAA OI SST V2 High-Resolution Data set (Reynolds et al., 2007; https://psl.noaa.gov/data/gridded/data.noaa.oisst.v2.highres.html). Wind speed data are from the ERA5 reanalysis data set (Hersbach et al., 2020; https://www.ecmwf.int/en/forecasts/datasets/reanalysis-datasets/era5). The pink dots mark core MD00-2354.

25724525, 2022, 10, Downloaded from https://agupubs.onlinelibrary.wiley.com/doi/10.1029/2022PA004453 by Cochrane France, Wiley Online Library on [27/11/2022]. See the Terms and Conditions (https://onlinelibrary.wiley.com/terms-and-conditions) on Wiley Online Library for rules of use; OA articles are governed by the applicable Creative Commons License

2.2. Coccolith Analysis

A total of 300 samples at 1 cm interval was analyzed at the Geoscience Paris-Saclay laboratory (Orsay, France) for coccolith data. This depth-spacing translates into resolutions ranging from ~20 to 100 years. The "settling" technique of Duchamp-Alphonse et al. (2018) modified after Beaufort et al. (2014) was used for preparing coccolith smear slides. Briefly, dry sediment was diluted in a high pH and bicarbonate rich water, ultra-sonicated and passed through a 20 µm cellulose membrane filter. The suspension was poured in a flat beaker for decantation on a coverslip, dried and mounted on a smear slide. This technique ensures an homogenous distribution of coccoliths and allow quantifying both, relative (%) and absolute abundances (number per gram of sediment) of specimens. For each slide, a total of at least 500 coccolith specimens was counted using a polarized light microscope (Leica DM6000B) at 1,000× magnification. The relative abundance (%) of coccolith species has been obtained as follows: Species% = 100 × (Species/total coccolith number). Particularly, the 95% confidence interval for Fp% was calculated following the method of Patterson and Fishbein (1984), and the errors are smaller than ±5%. We converted Fp% into PP by using the tropical Indian Ocean empirical equation proposed by Hernández-Almeida et al. (2019) as follow: PP (gC m^{-2} yr^{-1}) = [$10^{(3.27 - 0.01 \times Fp\%)}$] × 365/1,000. *C. leptoporus* absolute abundance has been calculated as follows: $A = (Nc \times Sf)/(No \times So \times Ws)$, where A is the absolute abundance (n/g of sediment), Nc is the number of counted *C. leptoporus* specimens; Sf is the surface of the flat beaker (diameter = 70 mm) in which suspended sediments (and total coccoliths) settled; No is the number of view fields; So is the surface of a view field (diameter = 0.25 mm); and Ws is the weight of sediment that settled in the flat beaker.

2.3. Climate Model and Simulations

2.3.1. IPSL-CM5A-LR

Paleoclimate simulations were run with the IPSL-CM5A coupled model (Dufresne et al., 2013), which has three model components: the LMDZ5A atmospheric general circulation model (Hourdin et al., 2013), the ORCHIDEE land surface model (Krinner et al., 2005), and the NEMO-PISCES ocean-biogeochemistry model (Aumont & Bopp, 2006; Madec, 2008). Simulations were run for the pre-industrial control (CTRL) in the framework of the Coupled Modeling Intercomparison Project phase 5 (Taylor et al., 2012) and for the LGM and the MH in the framework of Paleoclimate Modeling Intercomparison Project phase 3 (Braconnot et al., 2012). The comparison of LGM and MH mean states with CTRL are expressed in terms of differences (LGM–CTRL and MH–CTRL) to highlight specific atmospheric and oceanic responses under LGM and MH conditions. Compared to CTRL, MH is characterized by a smaller precession parameter, while larger ice sheets, lower greenhouse gases concentrations, and lower sea level are set for the LGM. Nutrient supplies from dust, rivers and sediments to the ocean are set to the CTRL values for all simulations (Kageyama, Braconnot, et al., 2013).

In brief, surface wind speed (m s^{-1}) and wind stress curl (N m^{-3}) were extracted to describe atmospheric conditions while surface nutrient content (mmol m^{-3}), mixed-layer depth (m), seawater vertical mass transport (upper 200 m mean, kg s^{-1}; Lee et al., 2000), together with temperature (°C), salinity (psu), and potential density (kg m^{-3}), were extracted to describe oceanic conditions. Temperature (salinity) vertical gradients were simplified by the difference between 0 (200 m) and 200 m (0 m) water depths, termed $\Delta T_{0-200\,m}$ ($\Delta S_{200-0\,m}$) in the following. The vertically averaged stable stability of the upper 200 m (termed $E_{0-200\,m}$, m^{-1}) represents the upper seawater stratification (Prasanna Kumar et al., 2002). Single layer stable stability (E) were calculated based on the normalized vertical density (ρ, kg m^{-3}) gradient: $E = -(1/\rho)\cdot(\partial\rho/\partial z)$, where z is the water depth (m). Variables used here are seasonally and annually averaged. Details of the model and the boundary conditions for these three experiments can be found in Dufresne et al. (2013) and Le Mézo et al. (2017).

2.3.2. TraCE-21

TraCE-21 is a transient simulation of the global climate evolution over the last 22 Kyr run with Community Climate System Model version 3 (Collins et al., 2006; Z. Liu et al., 2009). The simulation was initialized from a previous LGM equilibrium simulation of CCSM3 (Otto-Bliesner et al., 2006) and was then forced by a set of realistic transient climate forcing including orbital parameters, greenhouse gases concentrations, continental ice sheets, and glacial meltwater discharges. The last one can force the AMOC strength to change. Outputs of the single forcing experiments are also available (Z. Liu et al., 2009). We extracted annual mean temperature and salinity at 0 and 200 m and calculated annual mean vertically averaged stable stability of the upper 200 m ($E_{0-200\,m}$, m^{-1}) to describe oceanic conditions around site MD00-2354 (21°–23°N and 60°–68°E).

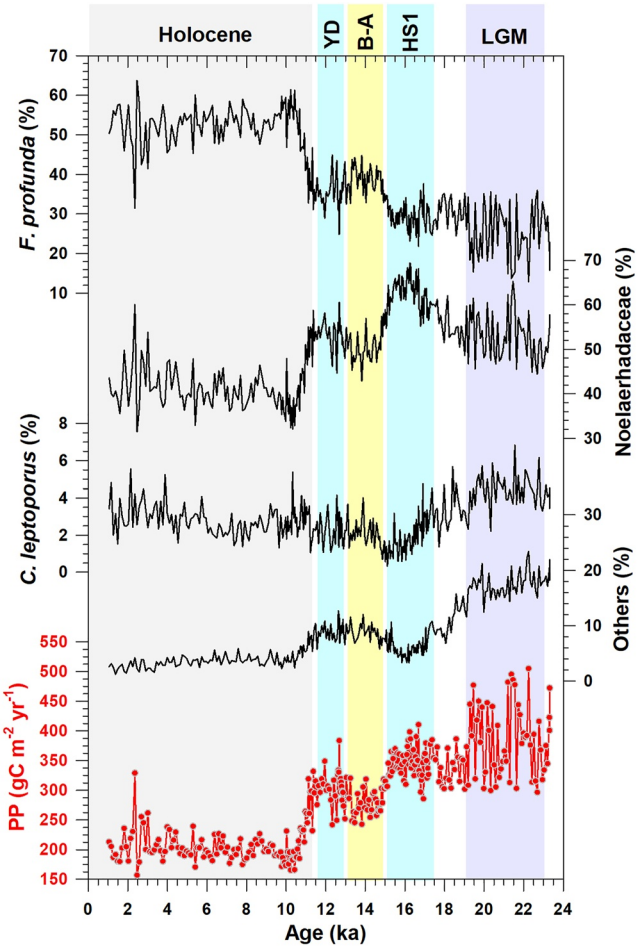

Figure 2. Relative abundance of the most significant contributors of the coccolith assemblage in core MD00-2354 (black), and quantitative primary productivity (PP; red) estimated by the Indian Ocean empirical equation of Hernández-Almeida et al. (2019). The detailed assemblage (i.e., the entire species %) is shown in Figure S2 in Supporting Information S1.

3. Results

3.1. Coccolith Assemblage and Reconstructed PP

At site MD00-2354, the Noelaerhabdaceae family (that includes *Emiliania huxleyi*, *Gephyrocapsa oceanica* and small *Gephyrocapsa*), together with *F. profunda,* represent more than 70% of the coccolith assemblage while *C. leptoporus*, *Umbilicosphaera* spp. and *Helicosphaera* spp. account for up to ~25% over the last ~23 Kyr (Figure 2 and Figure S2 in Supporting Information S1). Other species such as *Syracosphaera* spp. and *Rhabdosphaera* spp. are rare and altogether, never exceed 5%. Here, we focus on the Noelaerhabdaceae family and *F. profunda*, the most significant contributors of the assemblage, as well as *C. leptoporus* related to upwelling dynamic (Figure 2). Interestingly, *F. profunda* and the Noelaerhabdaceae depict opposite trends over the last 23 Kyr. While *F. profunda* shows a minimum (~15%) during the LGM, a two-step increase during the deglaciation, and a maximum (~60%) during the Holocene, the Noelaerhabdaceae show high values (~55%) during LGM, a two-step decrease during the deglaciation and a minimum (~25%) during the Holocene. During the deglaciation, millennial-scale variations of the Noelaerhabdaceae and *F. profunda* remain opposite. *F. profunda* (the Noelaerhabdaceae) shows averaged abundances of ~30% (~60%) and ~35% (~50%) during HS1 and YD and of ~39% (~54%) during B-A. *C. leptoporus* shows values as low as 0.5% during HS1 and depicts an increasing trend during the B-A with proportions as high as 2.5%.

Reconstructed PP varies between 150 and 500 gC m^{-2} yr^{-1} (Figure 2). Despite rather scattered values during the LGM, it appears that PP during this period (average of ~382 gC m^{-2} yr^{-1}; 23–19 ka) is about ~90% higher than during the Holocene (average of ~203 gC m^{-2} yr^{-1}; 11–0 ka). The maximum and minimum PP are found during the LGM and at 10 ka, respectively. During the deglaciation, PP averages are 346 and 305 gC m^{-2} yr^{-1} during HS1 and YD, and do not exceed 300 gC m^{-2} yr^{-1} during the B-A.

3.2. Simulated PP

Simulated PP obtained by IPSL-CM5A (CTRL, LGM–CTRL, and MH–CTRL) are shown in Figure 3. CTRL simulations show that the areas off Somalia-Oman and off Northern Oman and Pakistan, with PP as high as 400 gC m^{-2} yr^{-1}, are the most productive areas during preindustrial summer and winter, respectively, which is consistent with the VGPM modern features (Behrenfeld & Falkowski, 1997). The difference in annual PP between LGM and CTRL reveals a strong increase (>50 gC m^{-2} yr^{-1}) in the northern and northeastern parts of the basin and a strong decrease (<−50 gC m^{-2} yr^{-1}) along the coastal areas off Somalia and Oman. Such patterns are mainly related to winter conditions while the PP decrease in the western part may also be associated to the summer ones (Le Mézo et al., 2017). The difference in annual PP between MH and CTRL shows a general PP decrease over the basin. It is only in the northwestern AS off Oman that a PP increase (10–25 gC m^{-2} yr^{-1}) is simulated, as a result of a relatively high PP during summer (Le Mézo et al., 2017).

4. Discussion: Atmospheric and Oceanographic Implications Behind PP Patterns

4.1. Present Day Scenario

The modern seasonal pattern of PP simulated by CTRL in the studied area is shown in Figure 4. During summer, southwesterly winds alongshore Oman and Somalia, are accompanied by positive wind stress curl and upward seawater movements related to the coastal upwelling system. This mechanism increases the nutrient content in surface layers and results in relatively high PP. This high PP pattern is clearly not related to a weaker upper seawater stratification in the northwestern AS as no deeper mixed-layer, no decreased stable stability, and no

25724525, 2022, 10, Downloaded from https://agupubs.onlinelibrary.wiley.com/doi/10.1029/2022PA004453 by Cochrane France, Wiley Online Library on [27/11/2022]. See the Terms and Conditions (https://onlinelibrary.wiley.com/terms-and-conditions) on Wiley Online Library for rules of use; OA articles are governed by the applicable Creative Commons License

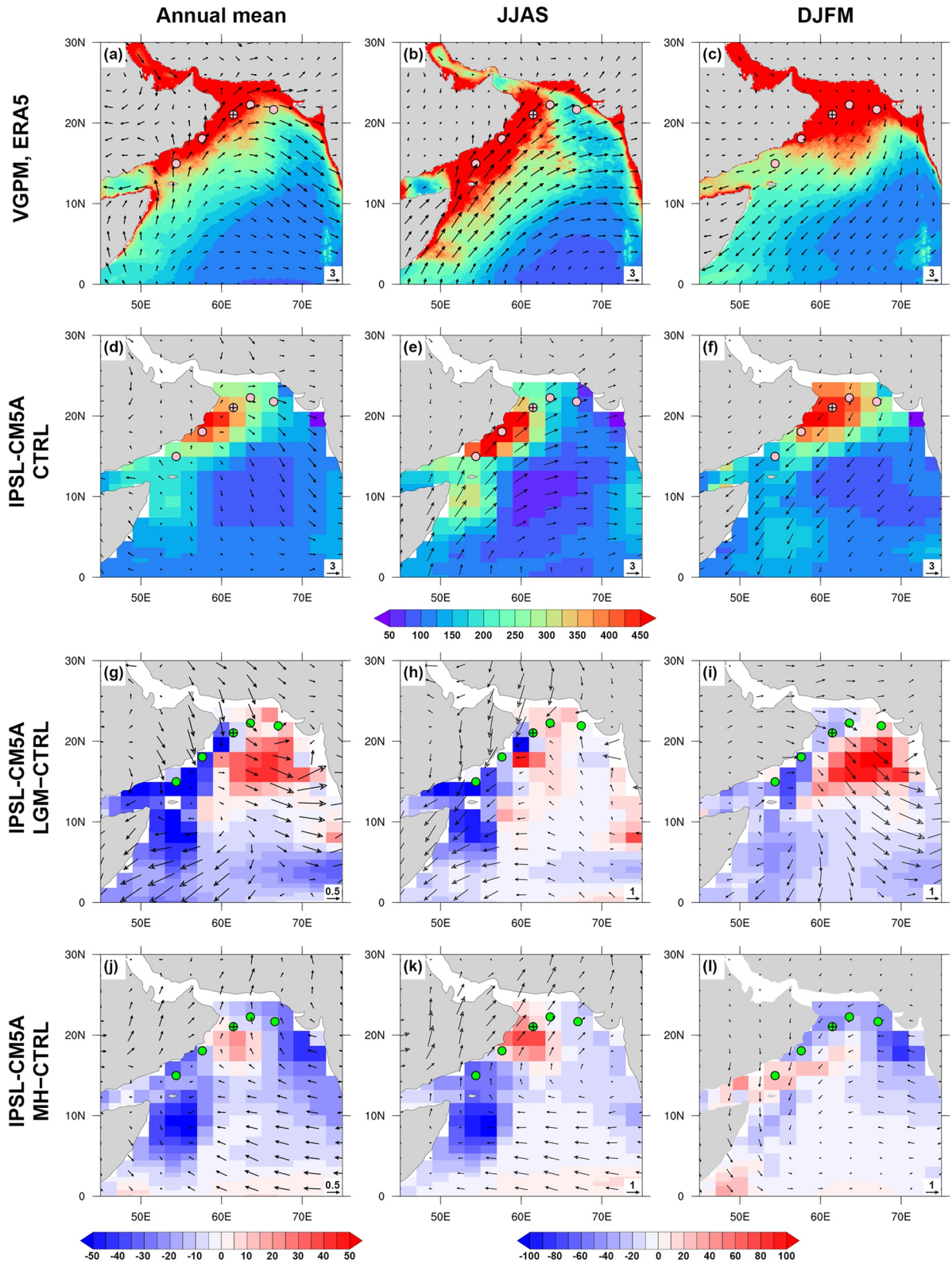

Figure 3.

25724525, 2022, 10, Downloaded from https://agupubs.onlinelibrary.wiley.com/doi/10.1029/2022PA004453 by Cochrane France, Wiley Online Library on [27/11/2022]. See the Terms and Conditions (https://onlinelibrary.wiley.com/terms-and-conditions) on Wiley Online Library for rules of use; OA articles are governed by the applicable Creative Commons License

25724525, 2022, 10, Downloaded from https://agupubs.onlinelibrary.wiley.com/doi/10.1029/2022PA004453 by Cochrane France, Wiley Online Library on [27/11/2022]. See the Terms and Conditions (https://onlinelibrary.wiley.com/terms-and-conditions) on Wiley Online Library for rules of use; OA articles are governed by the applicable Creative Commons License

smaller temperature and salinity gradients are simulated. During winter, no important positive wind stress curl and upwelling are found. Northeastern winds across AS are associated with a strong sea surface cooling in the northern part of the basin, which results in the collapse of the temperature vertical gradient and hence of the upper seawater stratification. These processes help sustaining a substantial amount of nutrients in the upper layers, which appears to drive high PP.

Despite the model being run at low resolution, the results of CTRL simulations document well the processes encountered in the upper layers of the AS during summer and winter seasons, processes by which, wind-driven coastal upwelling off Somalia and Oman, and surface cooling-driven convective mixing off North Oman and Pakistan drive high PP, respectively. They are also consistent with the findings of previous studies based on in-situ PP/chlorophyll-a and physical parameters data (e.g., Lee et al., 2000; Madhupratap et al., 1996; Prasanna Kumar, Madhupratap, et al., 2001). As a result, modern annual PP near site MD00-2354 is relatively important, as the surface ocean is under the direct influences of the two major seasonal phytoplankton blooms of the basin.

4.2. Glacial Condition Forcing During the LGM

Changes in PP, oceanographic and climate conditions in the AS over the last 23 Kyr are provided in Figure 5, based on new and published micropaleontological, geochemical and numerical data. The high PP signal (~380 gC m^{-2} yr^{-1}) obtained at site MD00-2354 mimics previous evidence of high PP (~500 gC m^{-2} yr^{-1}) at sites 94KL and ODP723A based on Fp% and indirectly at sites GeoB 3005 and NIOP464 based on TOC measurements, which reveals the occurrence of an extended high (exported-) PP cell in the northern and northwestern parts of the AS. Relatively low abundances of *C. leptoporus* (0.8 10^8 n/g) at site MD00-2354 coincide with relatively low percentage (~32%) of *G. bulloides* at site ODP723A, a planktonic foraminifer indicator for upwelling strength (Conan & Brummer, 2000; Curry et al., 1992). This indicates that higher PP in that area is not associated to the development of a strong upwelling system off Somalia and Oman, as the Indian summer monsoon was weaker than during the Holocene (Braconnot et al., 2007; Jiang et al., 2015; Kathayat et al., 2000). Such an interpretation is testified by the positive $\delta^{18}O$ anomalies obtained on speleothems from Moomi and Mawmluh caves, which indicate relatively low Indian summer monsoon moisture transport and rainfall. It is also supported by the positive seawater $\delta^{18}O$ anomalies from site 126KL (northern Bay of Bengal), which documents relatively high sea surface salinity. In parallel, the relatively cold alkenone-based SST data from core 136KL located in the northeastern AS, away from the coastal upwelling area, show that forcing factors driving this higher PP cell might be found within mechanisms involving cooling-driven convective mixing and a weaker stratification in the euphotic zone. Such an interpretation is testified by TraCE that simulates the exact same SST trends as those obtained at site 136KL and depicts relatively low annual mean seawater stratification in the northern AS, due to a smaller vertical temperature gradient rather than a smaller salinity one (Figures 5b and 6). It is also well expressed by IPSL-CM5A. Even if the model simulates a summer season with anomalous northeasterly winds along the coastal area off Somalia and Oman that drive positive wind stress curl anomalies over the western AS and a slight increase of PP, it clearly appears that the summer monsoon is reduced and that annual mean conditions (and thus PP patterns), reflect a stronger winter one (Figures 3 and 7). High PP in the northern AS are driven by strong northwesterly winds which, together with a smaller vertical SST gradient, generate a weaker stratification and higher nutrient contents in surface layers (Figures 3 and 7). Overall, such scenario is consistent with extended ice sheets and lower greenhouse gas concentration that characterize the LGM (Joos & Spahni, 2008; Peltier, 2004; Tierney et al., 2020). As the global annual cooling occurred during the LGM with a strongest impact over the ice sheet regions than the tropics (Shakun et al., 2012; Tierney et al., 2020), it drove a stronger and weaker temperature contrast between Eurasia and northern Indian Ocean during winter and summer, respectively, and thus, a weaker summer monsoon and a stronger winter monsoon over the AS (Böll et al., 2015; Braconnot et al., 2007; Jiang et al., 2015; Reichart et al., 2004; Tian & Jiang, 2016).

Figure 3. (a–c) Annual mean (ANN), summer (June–July–August–September, JJAS), and winter (December–January–February–March, DJFM) integrated primary productivity (PP; gC m^{-2} yr^{-1}) calculated by VGPM model based on MODIS chlorophyll concentration data (Behrenfeld & Falkowski, 1997) and surface wind (m s^{-1}) in the ERA5 reanalysis data set. (d–f) Annual mean, summer, and winter integrated PP and surface wind simulated by CTRL experiment of IPSL-CM5A. (g–i) Differences of annual mean, summer, and winter integrated PP and surface wind between Last Glacial Maximum and CTRL experiments of IPSL-CM5A. (j–l) Differences of annual mean, summer, and winter integrated PP and surface wind between Mid-Holocene (MH) and CTRL experiments of IPSL-CM5A. The dots mark the locations of cores MD00-2354 (dots with inside crosses), OPD723A, NIOP464, GeoB 3005, and 94KL (see Figure 1a) with published indirect PP data (shown in Figure 5).

10.1029/2022PA004453

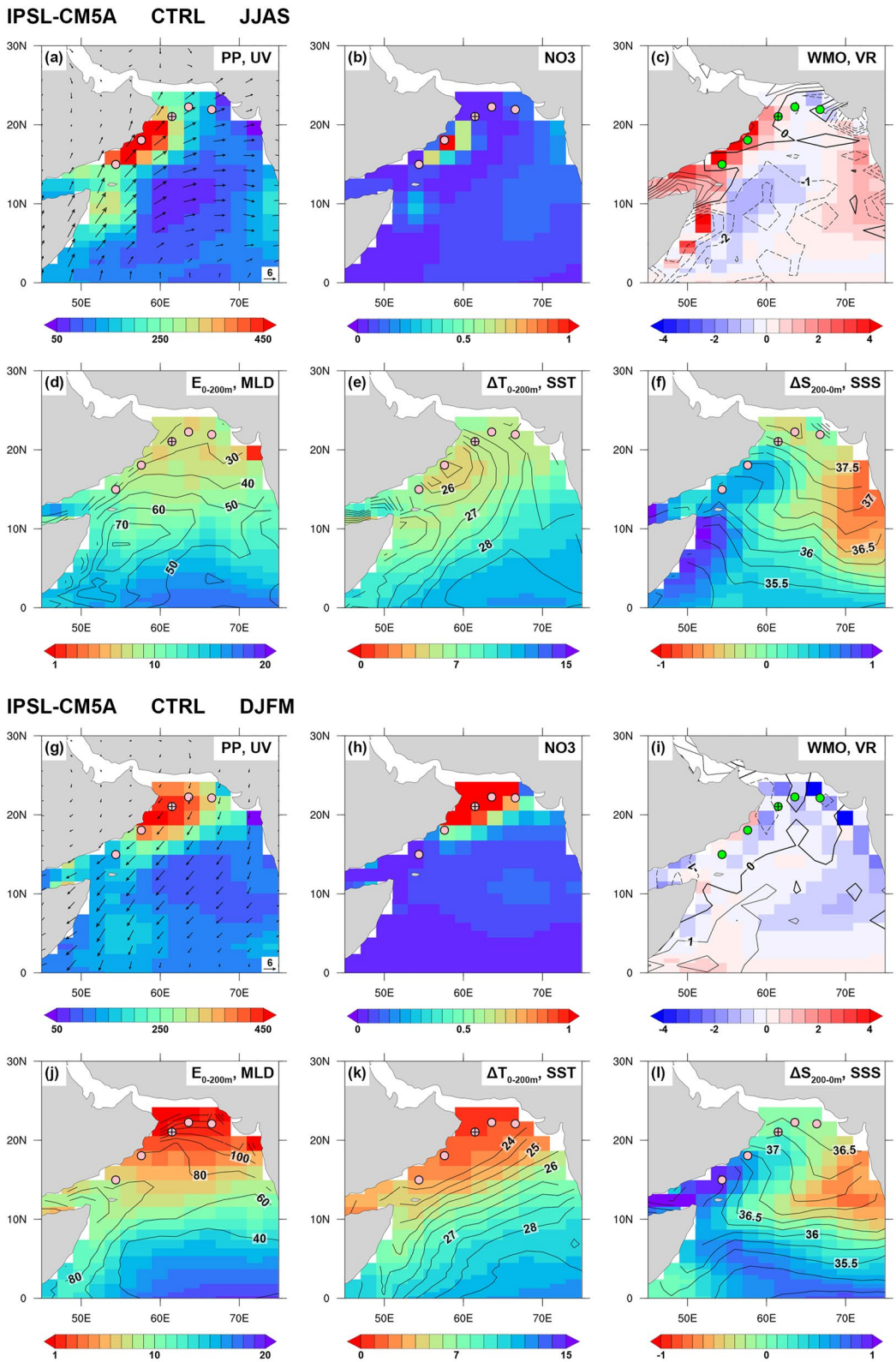

Figure 4.

25724525, 2022, 10, Downloaded from https://agupubs.onlinelibrary.wiley.com/doi/10.1029/2022PA004453 by Cochrane France, Wiley Online Library on [27/11/2022]. See the Terms and Conditions (https://onlinelibrary.wiley.com/terms-and-conditions) on Wiley Online Library for rules of use; OA articles are governed by the applicable Creative Commons License

25724525, 2022, 10, Downloaded from https://agupubs.onlinelibrary.wiley.com/doi/10.1029/2022PA004453 by Cochrane France, Wiley Online Library on [27/11/2022]. See the Terms and Conditions (https://onlinelibrary.wiley.com/terms-and-conditions) on Wiley Online Library for rules of use; OA articles are governed by the applicable Creative Commons License

Such conditions are confirmed by ^{230}Th-normalized detrital flux records at sites 93KL and RC-27-42 that show, despite low time resolution, that aeolian inputs were higher in the northern and western AS, in conjunction with higher PP during the LGM. Following Tamburini et al. (2003), it is most probable that enhanced fertilization by aeolian input due to increased aridity on the adjacent continents account for a part of the high PP signal obtained at that time (Pourmand et al., 2004, 2007). Glacial conditions do promote the increase of global dust emission and deposition (e.g., Albani et al., 2016, 2018; Lambert et al., 2013; Lamy et al., 2014; Maher et al., 2010; Martínez-García et al., 2009; Winckler et al., 2008) and this is particularly the case during the LGM (Sirocko et al., 1991, 2000). Guieu et al. (2019) demonstrated, based on sensitivity experiments of dust deposition run with a coupled model, that null dust accumulation in the AS could reduce PP by 50%. Following their findings and if the response is linear, the ∼40% stronger aeolian flux recorded during the LGM relative to the Holocene (Figures 5q and 5r) could increase PP by ∼20%, thus explaining a part of the recorded ∼90% higher PP signal.

In summary, the high PP observed in the northwestern part of the basin during the LGM most likely reflects higher nutrient inputs in the euphotic zone due to the combined effects of stronger surface cooling-driven mixing and stronger aeolian input. They resulted from both, stronger winter and weaker summer monsoon conditions.

4.3. Glacial Waning and AMOC Forcing During the Last Deglaciation

On the long term (between 19 and 10 ka), the decreasing trend of PP (from ∼380 to 200 gC m^{-2} yr^{-1}) and the increasing trend of *C. leptoporus* abundance (from 0.8 to 1.2 10^8 n/g) obtained at site MD00-2354, mimic Fp%-PP, TOC and *G. bulloides* signals previously obtained in the studied area (Figure 5). These results indicate that during the deglaciation, reducing PP in the northwestern part of the AS is associated with intensifying coastal upwelling off Somalia-Oman and strengthening summer monsoon. In parallel, rising SST are recorded at sites 136KL and MD00-2354 and simulated by TraCE in conjunction with rising stratification in the upper layers (Figure 5). This highlights a reduction of the surface cooling-driven convective mixing, compatible with a weakening of the winter monsoon. These findings are in agreement with the $\delta^{18}O_{speleothem}$ signals obtained in Moomi and Mawmluh caves and the SSS record from the northern Bay of Bengal, that point to a transition from cold and dry conditions during the LGM, to warm and wet ones during the early Holocene, as the summer monsoon strengthens. This is expected when increased Northern Hemisphere summer insolation, smaller ice sheets and increased atmospheric greenhouse gas concentration, induce faster warming of Eurasia with respect to the northern Indian ocean (e.g., Blaga et al., 2013; Cheng et al., 2016; Clark et al., 2012; Joos & Spahni, 2008; Peltier, 2004; Renssen & Isarin, 2001; Shakun et al., 2012; Sowers & Bender, 1995; Tierney et al., 2008). These findings also show that PP patterns that document an overall decrease in upper layer nutrient contents in the northern AS are rather sensitive to the weakening of the surface cooling-driven convective mixing than the strengthening of the wind-driven coastal upwelling. The long-term decreasing trends in PP also match the long-term decreasing trends in the ^{230}Th-normalized detrital flux. Therefore, it is most possible that the concomitant reduction in the aeolian dust activity and hence, in dust-derived nutrients in surface waters, also contributed in driving the overall decrease in PP during the deglaciation relative to the LGM.

On millennial-scale, PP and *C. leptoporus* records obtained at site MD00-2354 between 19 and 10 ka, highlight HS1, B-A and YD climate periods that is, the three stages that correspond to significant changes in the AMOC strength (Figure 5). During the cold HS1 and YD periods relatively high PP signals are accompanied by relatively low *C. leptoporus* abundances while opposite trends are recorded during the warm B-A. Therefore, in a similar way as for the long-term trends, high PP characterizes periods when the coastal upwelling off Oman weakened and when SST in the northern AS decreased. TraCE, which is forced by high latitude melt water fluxes (AMOC strength) during the deglaciation in addition to long-term changes in insolation, greenhouse gases and ice sheets (Figure S3 in Supporting Information S1), simulates a weaker upper seawater stratification due to lower SST and hence, stronger surface cooling-driven convective mixing during HS1 and YD, while opposite conditions

Figure 4. Analysis of primary productivity (PP) using CTRL outputs of IPSL-CM5A in (a–f) summer (JJAS) and (g–l) winter (DJFM). (a and g) Integrated PP (color, gC m^{-2} yr^{-1}) and surface wind (vectors, m s^{-1}). (b and h) Surface concentration of nitrate (NO_3, mmol m^{-3}). (c and i) Vertically averaged mass transport of the upper 200 m seawater (WMO, color, kg s^{-1}) and wind stress curl (VR, contours, 10^7 N m^{-3}). (d and j) Upper seawater stratification quantified by vertically averaged stable stability of the upper 200 m ($E_{0-200\,m}$, color, 10^6 m^{-1}) and mixed-layer depth (MLD; contours, m). (e and k) Upper seawater temperature gradient quantified by the difference between the surface and 200 m ($\Delta T_{0-200\,m}$, color, °C) and sea surface temperature (SST, contours, °C). (f and l) Upper seawater salinity gradient quantified by the difference between 200 m and the surface ($\Delta S_{200-0\,m}$, color, psu) and sea surface salinity (SSS, contours, psu). The dots have the same representations as those in Figure 3.

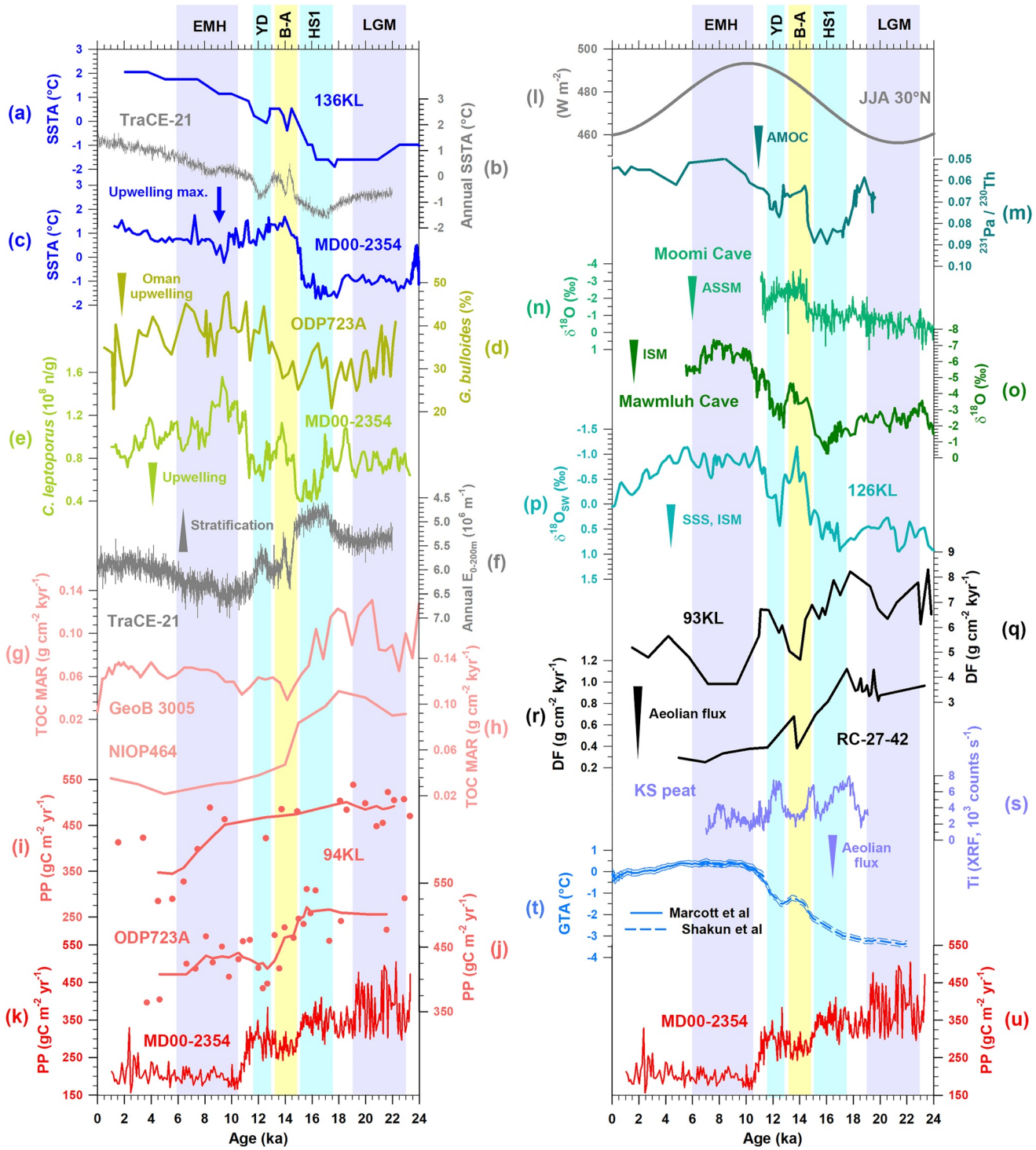

Figure 5.

are simulated during the B-A (Figures 5 and 6). More precisely, results for HS1 versus B-A events show that HS1, as defined by a weakened AMOC, is characterized by annual mean anomalous northerly winds, together with weaker temperature-related stratification over the AS compared to B-A (Figure 6). Therefore, it appears that high PP and weakened coastal upwelling off Oman occur when stronger (weaker) Indian winter (summer) monsoon conditions prevailed, and vice versa. Compared to the temperature vertical gradient in the upper waters,

25724525, 2022, 10, Downloaded from https://agupubs.onlinelibrary.wiley.com/doi/10.1029/2022PA004453 by Cochrane France, Wiley Online Library on [27/11/2022]. See the Terms and Conditions (https://onlinelibrary.wiley.com/terms-and-conditions) on Wiley Online Library for rules of use; OA articles are governed by the applicable Creative Commons License

25724525, 2022, 10, Downloaded from https://agupubs.onlinelibrary.wiley.com/doi/10.1029/2022PA004453 by Cochrane France, Wiley Online Library on [27/11/2022]. See the Terms and Conditions (https://onlinelibrary.wiley.com/terms-and-conditions) on Wiley Online Library for rules of use; OA articles are governed by the applicable Creative Commons License

the salinity gradient has limited variations and a weak control on the upper seawater stratification (Figure 6 and Figure S4 in Supporting Information S1). This is reflected by the much stronger correlation between the temperature gradient and stratification over the deglaciation (Figure S4 in Supporting Information S1). These variations of the upper seawater stratification demonstrate the control millennial-scale changes in the AMOC state (high-latitude) exerts on the AS conditions and PP distribution (low-latitude) (Ivanochko et al., 2005; Kageyama, Merkel, et al., 2013; Marzin et al., 2013; Obase & Abe-Ouchi, 2019; Schulz et al., 1998; Shakun et al., 2007; Z. Liu et al., 2009). According to Marzin et al. (2013), a weakened AMOC can drive a reduction of the temperature gradient between Euro-Asia and the Indian Ocean, a southward shift of the Intertropical Convergence Zone, and a weaker Indian summer monsoon. However not much is known about millennial-scale changes of the Indian winter monsoon during the last deglaciation (Böll et al., 2015). Wen et al. (2016) proposed that the East Asian winter monsoon became stronger during HS1 and the YD and was therefore anti-phased with the East Asian summer monsoon. Here, our results are consistent with such an anti-phased pattern. Weaker AMOC during HS1 and YD reduced the annual northward heat transport from the tropical Atlantic and resulted in Eurasian cooling throughout the year. It therefore reduced and enhanced the land-sea temperature gradients over the Indian monsoon region during summer and winter, respectively, and thus, drove a weaker summer monsoon and a stronger winter one while opposite conditions are recorded during the B-A (Wen et al., 2016; Figure S5 in Supporting Information S1). Different from the East Asian, the winter monsoon over the AS might be more directly influenced by the cooling over the subtropical Mid-East and Tibetan plateau than the Mongolia-Siberian high-pressure cell (Chang et al., 2006; Goes et al., 2020; Y. Liu et al., 2020). However, further data of sensitivity modeling experiments are required to better understand the connexions of the Indian winter monsoon with the AMOC.

At last, since PP changes in concert with ^{230}Th-normalized detrital flux in the northern AS and with Ti_{XRF} signal in the southeastern Iran (Figure 5), one cannot exclude that dust storms contributed in shaping millennial-scale PP patterns as well. In that scenario, more (less) frequent and/or stronger (weaker) dust storms during HS1 and YD (B-A) that is, when continental aridity increases (reduces), would provide higher (lower) bioavailable nutrients to PP in this area. Indeed, one could have expected an increase of PP during the last deglaciation as SST raised and the coastal upwelling off Somalia and Oman reinforced. However, it clearly appears that fertilization of the euphotic zone due to stronger winter monsoon conditions and higher aeolian inputs, is much more efficient on annual PP than is the summer monsoon-driven upwelling.

4.4. Precession Forcing During the Holocene

Values of PP (average of ~200 gC m^{-2} yr^{-1}) and TOC obtained at sites MD00-2354, GEOB 3005 and NIOP464, together with values of *C. leptoporus* (1.2 10^9 n/g) and *G. bulloides* abundances obtained at sites MD00-2354 and ODP723A, respectively, show that the Holocene is characterized by the lowest PP in northern AS, and the strongest coastal upwelling off Somalia-Oman over the past 23 Kyr (Figure 5). Together with relatively high SST at sites 136KL and relatively low SSS at site 126KL, they show that warm and humid conditions installed and document that summer monsoon intensified as winter monsoon weakened compared to the glacial period

Figure 5. (a) Alkenone-derived sea surface temperature (SST) anomalies in core 136KL (Schulte & Müller, 2001). (b) Annual mean SST anomalies in the northern Arabian Sea (AS) (21°–23°N and 60°–68°E; AS) simulated by TraCE-21. (c) Alkenone-derived SST anomalies in core MD00-2354 (Böll et al., 2015). (d) Relative abundance of *G. bulloides* in core OPD723A indicating the variations of Oman upwelling intensity (Naidu & Malmgren, 1996). (e) Absolute abundance (n/g) of *Calcidiscus leptoporus* in core MD00-2354 (5-point moving average). (f) Annual mean seawater stratification in the northwestern AS simulated by TraCE-21. Mass accumulation rates (MAR) of total organic carbon (TOC) of cores (g) GeoB 3005 from the western AS (Budziak et al., 2000) and (h) NIOP464 from the northern AS (Reichart et al., 1997). Reconstructed primary productivity (PP) in (i) core 94KL (northern AS) and (j) core ODP723A (western AS) based on *Florisphaera profunda* percentages from Rogalla and Andruleit (2005) using the same PP empirical equation (Hernández-Almeida et al. (2019) as that for core MD00-2354. The lines show the results of three-point moving average. (k) Reconstructed PP in core MD00-2354 (this study). (l) Summer (June-July-August) insolation at 30°N (Laskar et al., 2004). (m) Atlantic Meridional Overturning Circulation strength revealed by the ^{231}Pa/^{230}Th ratio in marine sediments from the western subtropical Atlantic Ocean (McManus et al., 2004). (n) Speleothem δ^{18}O record from the Moomi Cave indicating the variations of summer moisture transport over the western AS (Shakun et al., 2007). (o) Speleothem δ^{18}O record from the Mawmluh Cave indicating the variations of Indian summer monsoon rainfall (Dutt et al., 2015). (p) Seawater δ^{18}O record of core 126KL indicating the variations of sea surface salinity and Indian summer monsoon rainfall (Kudrass et al., 2001). ^{230}Th-normalized detrital flux of core (q) 93KL from the northern AS (Pourmand et al., 2004) and (r) core RC-27-24 from the western AS (Pourmand et al., 2007), both indicating aeolian dust flux. (s) Downcore Ti abundance measured by XRF of a sediment core from the Konar Sandal peat bog, southeastern Iran (Safaierad et al., 2020). (t) Global mean surface temperature anomalies referenced to the period of 1961–1990 (Marcott et al., 2013; Shakun et al., 2012). The data of Shakun et al. was aligned to that of Marcott et al.'s. The thin curves represent 1σ. (u) Reconstructed PP in core MD00-2354 (this study).

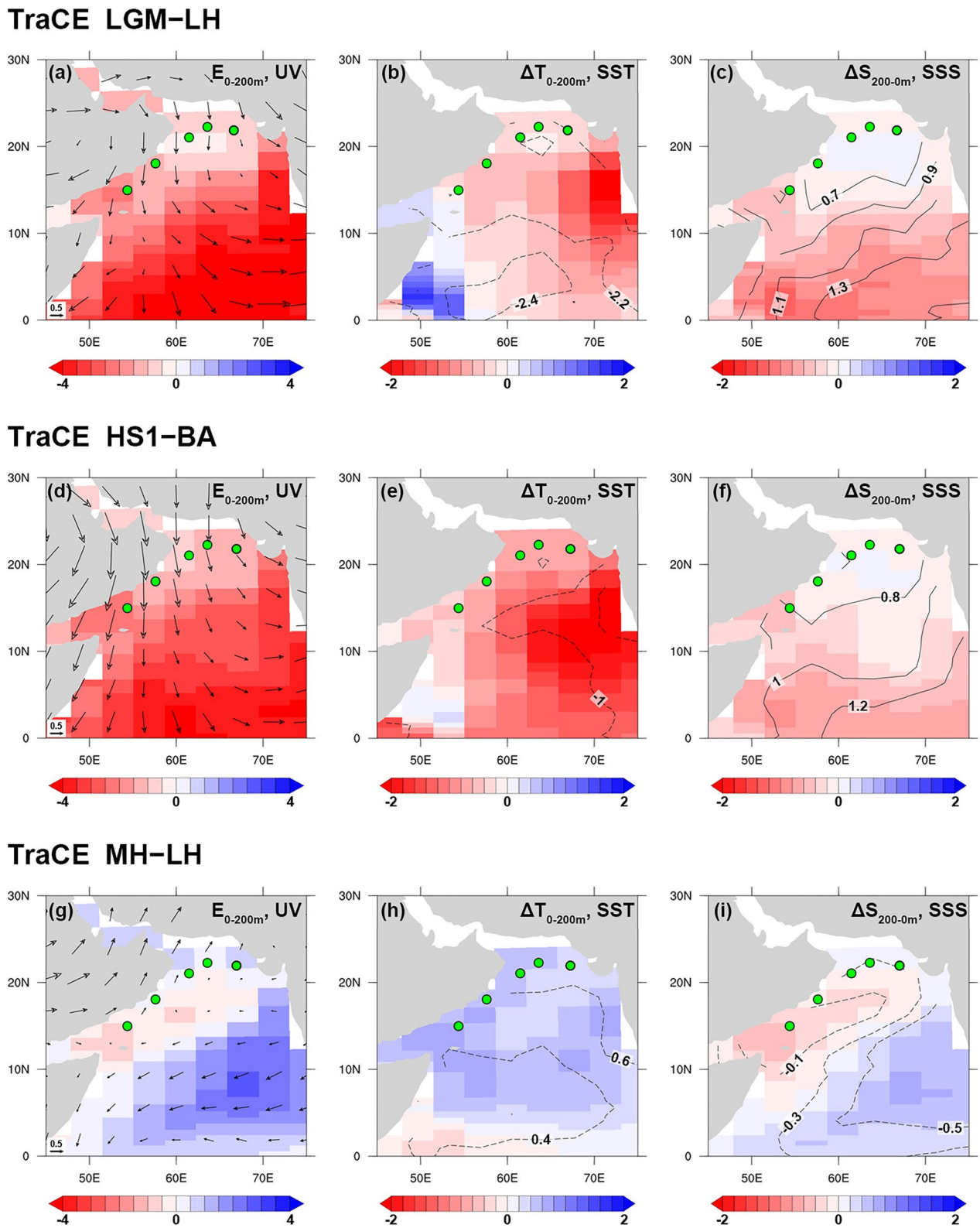

Figure 6. Differences of annual mean $E_{0-200\,m}$ (10^6 m^{-1}), surface wind (vectors, m s^{-1}), $\Delta T_{0-200\,m}$ (°C), and $\Delta S_{200-0\,m}$ (psu) between (a–c) Last Glacial Maximum (LGM; 21.5–21 ka) and late-Holocene (LH; 1–0 ka), between (d–f) HS1 (17–15.5 ka) and BA (14.7–13 ka), and between (g–i) Mid-Holocene (MH; 6.5–6 ka) and LH of TraCE-21.

25724525, 2022, 10, Downloaded from https://agupubs.onlinelibrary.wiley.com/doi/10.1029/2022PA004453 by Cochrane France, Wiley Online Library on [27/11/2022]. See the Terms and Conditions (https://onlinelibrary.wiley.com/terms-and-conditions) on Wiley Online Library for rules of use; OA articles are governed by the applicable Creative Commons License

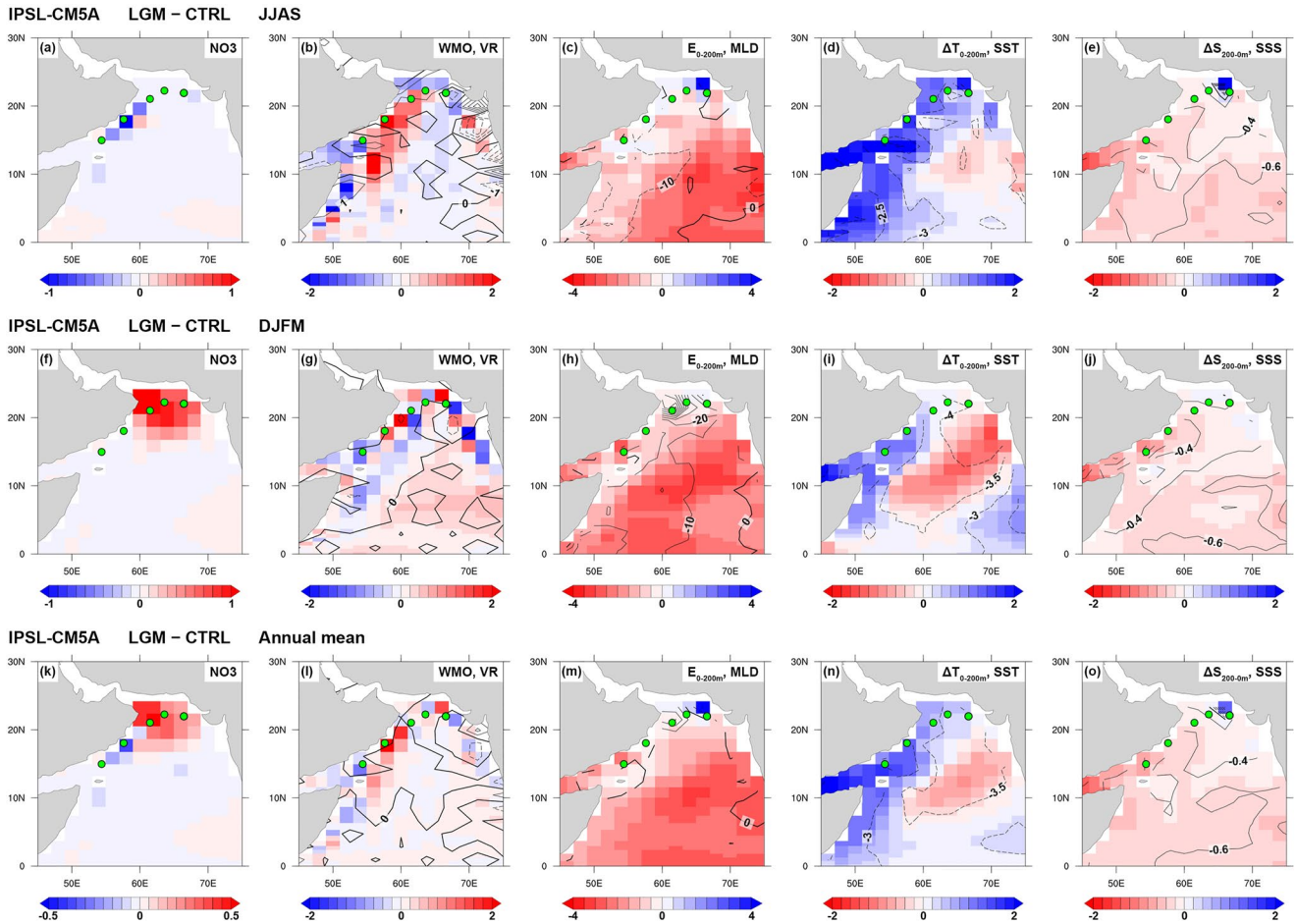

Figure 7. Differences between Last Glacial Maximum (LGM) and CTRL experiments of IPSL-CM5A-LR in (a–e) summer, (f–j) winter, and (k–o) annual mean. The parameters are the same as those in Figure 4.

(Figures 3 and 7). In parallel, the relatively low ^{230}Th-normalized detrital flux documents a reduction in aeolian inputs with a probable impact on PP.

In detail, despite rather scattered values, it appears that PP and *C. leptoporus* reach minima and maxima values during the Early-Mid Holocene (EMH; 10–8 ka), before showing slightly increasing and decreasing trends up to the late Holocene (2 ka), respectively (Figure 5). These results are consistent with TOC, *G. bulloides* and MD00-2354 SST records indicating PP minimum and upwelling maximum at EMH (Figure 5), as well as with the aforementioned PP and climate data, that testify for slightly lower annual PP and stronger coastal upwelling dynamics off Oman and Somalia during the EMH (e.g., Gupta et al., 2003; Ivanochko et al., 2005). Such patterns are expressed by TraCE and IPSL-CM5A with MH–LH and MH–CTRL experiments, respectively. Indeed, despite nearly unchanged upper layer stratification due to nearly unchanged temperature and salinity gradients along Somalia and Oman, the imprint of stronger summer monsoon during MH is seen in the annual mean simulations that are characterized by stronger southwesterly winds (Figures 3 and 8). Interestingly, such conditions are not associated with a strong increase of nutrient and hence PP, in surface waters (Figure 8), because the negative wind stress curl anomalies, simulated during summer in the western AS, limits the advection of the coastal upwelling off Somalia and Oman (Le Mézo et al., 2017). In parallel, the winter season is characterized by slightly stronger northeasterly winds and slightly lower PP in the northern AS (Figure 3), with limited changes in upper layer temperature- or salinity-related stratification, and no significant impact on the annual mean setting (Figure 8). Overall, simulations are in good agreement with a smaller precession parameter during the EMH that results in both, stronger summer and winter monsoons due to enhanced summer and lower winter insolation, respectively (Wen et al., 2016), but with a more important imprint of summer monsoon on the annual mean. Such

25724525, 2022, 10, Downloaded from https://agupubs.onlinelibrary.wiley.com/doi/10.1029/2022PA004453 by Cochrane France, Wiley Online Library on [27/11/2022]. See the Terms and Conditions (https://onlinelibrary.wiley.com/terms-and-conditions) on Wiley Online Library for rules of use; OA articles are governed by the applicable Creative Commons License

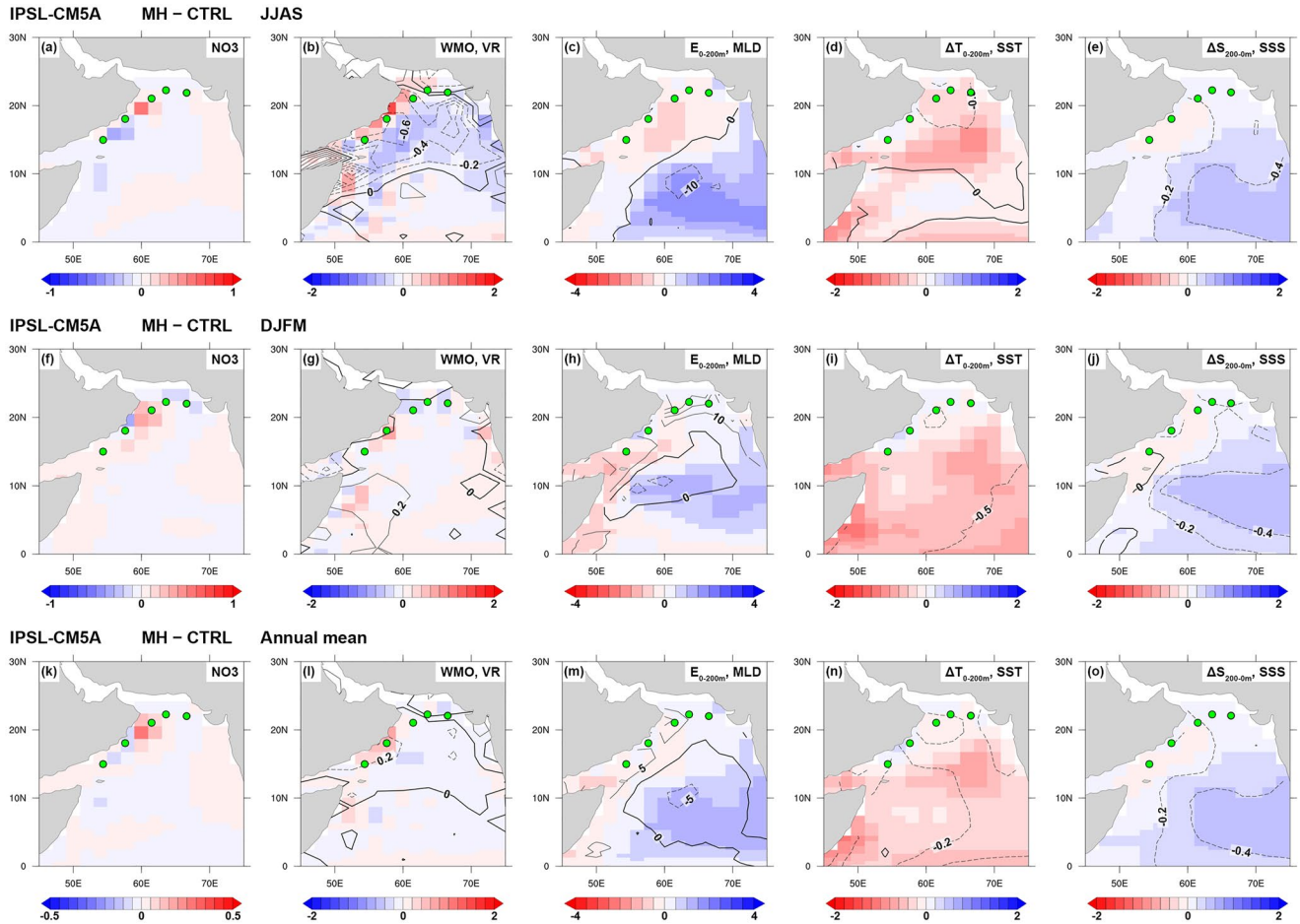

Figure 8. Differences between Mid-Holocene (MH) and CTRL experiments of IPSL-CM5A-LR in (a–e) summer, (f–j) winter, and (k–o) annual mean. The parameters are the same as those in Figure 4.

trends are also well expressed by the ^{230}Th-normalized detrital flux recorded in the northern AS that documents minimum aeolian input during the EMH (Figure 5l) and probably reflect wettest climate and densest vegetation cover around the AS (Davies, 2006; Engel et al., 2012; Hoelzmann et al., 1998; Jiménez-Espejo et al., 2014; Kuper & Kröpelin, 2006; Swann et al., 2014). In such a scenario, it appears that the EMH annual PP minimum recorded in the northwestern AS results from (a) restricted extension of coastal upwelling cell due to the negative wind stress curl anomalies, (b) limited strengthening in the convective mixing associated to the slight increase of winter wind intensity, and (c) weaker aeolian input associated to a wetter period. Further model-data comparisons on the AS are needed to better unravel the impact the summer versus winter monsoons exert on PP during the Holocene and particularly during EMH.

5. Conclusions

We provide for the first time, high-resolution PP and coastal upwelling dynamic records of the northwestern AS over the last 23 Kyr, based on coccolith assemblages from the sediment core MD00-2354. Comparisons of these signals with previous micropalaeontological and geochemical data and new model outputs help us to evaluate the impact of summer and winter Indian monsoons, as well as aeolian dust inputs, on PP. We demonstrate that changes in the surface cooling-driven mixing (winter monsoon), together with changes in aeolian inputs, have a greater impact on nutrient budget in the euphotic and hence PP, than changes in the coastal upwelling (summer monsoon). Thus, this study questions the usual paradigm that PP distribution in the (north-) western AS is necessarily shaped by changes in summer monsoon. Higher PP during the LGM relative to the Holocene resulted from the increase of nutrient concentration in surface layers due to the strengthening of both, surface cooling-driven

25724525, 2022, 10, Downloaded from https://agupubs.onlinelibrary.wiley.com/doi/10.1029/2022PA004453 by Cochrane France, Wiley Online Library on [27/11/2022]. See the Terms and Conditions (https://onlinelibrary.wiley.com/terms-and-conditions) on Wiley Online Library for rules of use; OA articles are governed by the applicable Creative Commons License

25724525, 2022, 10, Downloaded from https://agupubs.onlinelibrary.wiley.com/doi/10.1029/2022PA004453 by Cochrane France, Wiley Online Library on [27/11/2022]. See the Terms and Conditions (https://onlinelibrary.wiley.com/terms-and-conditions) on Wiley Online Library for rules of use; OA articles are governed by the applicable Creative Commons License

mixing and aeolian activity as the winter monsoon was stronger and the summer monsoon was weaker. Similar conditions are recorded during the HS1 and YD cold periods, when weaker AMOC conditions reinforced winter monsoon conditions. Lower PP are recorded during the warm B-A and the Holocene despite the reinvigoration of the coastal upwelling off Somalia and Oman under stronger summer monsoon conditions. Such patterns result from weaker winter monsoon conditions that are accompanied by a weaker surface cooling-driven mixing, a reduction of aeolian activity and overall, lower nutrient inputs in ocean surface layers. Over the Holocene, PP was minimum during the EMH, despite stronger summer and winter monsoon conditions. This is due to the combination of restricted advection of summer upwelling cell under negative wind stress curls with limited winter mixing and lower aeolian input.

Data Availability Statement

Coccolith and estimated PP data of core MD00-2354 are available in the PANGAEA data repository (Zhou et al., 2022). The data of Last Glacial Maximum, Mid-Holocene, and CTRL experiments of IPSL-CM5A-LR model are respectively available through Kageyama et al. (2016), Braconnot et al. (2016), and Caubel et al. (2016), respectively. The data of TraCE-21 simulation and the single forcing experiments are available in the Earth System Grid of the National Center for Atmospheric Rearch (https://www.earthsystemgrid.org/project/trace.html; Z. Liu et al., 2009).

Acknowledgments
The simulations presented in this work have been run on the TGCC (Très Grand Centre de Calcul du CEA) supercomputing equipment under the gen2212 project, provided by GENCI (Grand Equipment National de Calcul Intensif). The authors would like to thank the Institut Pierre Simon Laplace (IPSL) and the researchers who developed the IPSLCM5A model, those who ran the model for the Coupled Modeling Intercomparison Project phase 5 and Paleoclimate Modeling Intercomparison Project phase 3, and the TraCE-21 group for sharing the modelling output via the Earth System Grid of the National Center for Atmospheric Research. The authors wish to thank the on-board scientists of *R.V. Marion Dufresne* in 2000 for retrieving sediment core MD00-2354. Xinquan Zhou thanks the China Scholarship Council for providing him a PhD grant at the Geoscience Paris-Saclay laboratory (Paris Saclay University). The authors also thank the editors and the two anonymous reviewers for their constructive remarks.

References

Albani, S., Balkanski, Y., Mahowald, N., Winckler, G., Maggi, V., & Delmonte, B. (2018). Aerosol-climate interactions during the Last Glacial Maximum. *Current Climate Change Reports*, *4*(2), 99–114. https://doi.org/10.1007/s40641-018-0100-7

Albani, S., Mahowald, N. M., Murphy, L. M., Raiswell, R., Moore, J. K., Anderson, R. F., et al. (2016). Paleodust variability since the Last Glacial Maximum and implications for iron inputs to the ocean. *Geophysical Research Letters*, *43*(8), 3944–3954. https://doi.org/10.1002/2016GL067911

Anderson, D. M., & Prell, W. L. (1993). A 300 kyr record of upwelling off Oman during the Late Quaternary: Evidence of the Asian Southwest Monsoon. *Paleoceanography*, *8*(2), 193–208. https://doi.org/10.1029/93PA00256

Andruleit, H., & Rogalla, U. (2002). Coccolithophores in surface sediments of the Arabian Sea in relation to environmental gradients in surface waters. *Marine Geology*, *186*(3–4), 505–526. https://doi.org/10.1016/S0025-3227(02)00312-2

Andruleit, H., Rogalla, U., & Stäger, S. (2004). From living communities to fossil assemblages: Origin and fate of coccolithophores in the northern Arabian Sea. *Micropaleontology*, *50*(S1), 5–21. https://doi.org/10.2113/50.Suppl_1.5

Andruleit, H., Stäger, S., Rogalla, U., & Cepek, P. (2003). Living coccolithophores in the northern Arabian Sea: Ecological tolerances and environmental control. *Marine Micropaleontology*, *49*(1–2), 157–308. https://doi.org/10.1016/S0377-8398(03)00049-5

Andruleit, H. A., von Rad, U., Bruns, A., & Ittekkot, V. (2000). Coccolithophores fluxes sediment traps in the northeastern Arabian Sea off Pakistan. *Marine Micropaleontology*, *38*(3–4), 285–308. https://doi.org/10.1016/S0377-8398(00)00007-4

Aumont, O., & Bopp, L. (2006). Globalizing results from ocean in situ iron fertilization studies. *Global Biogeochemical Cycles*, *20*(2), GB2017. https://doi.org/10.1029/2005GB002591

Balaji, D., Bhushan, R., & Chamyal, L. S. (2018). Variations of the Somali upwelling since 18.5 ka BP and its relationship with southwest monsoon rainfall. *Climate of the Past*, *14*(9), 1331–1343. https://doi.org/10.5194/cp-14-1331-2018

Bali, K., Mishra, A. K., Singh, S., Chandra, S., & Lehahn, Y. (2019). Impact of dust storm on phytoplankton bloom over the Arabian Sea: A case study during March 2012. *Environmental Science and Pollution Research*, *26*(12), 11940–11950. https://doi.org/10.1007/s11356-019-04602-7

Banerjee, P., & Prasanna Kumar, S. (2014). Dust-induced episodic phytoplankton blooms in the Arabian Sea during winter monsoon. *Journal of Geophysical Research: Oceans*, *119*(10), 7123–7138. https://doi.org/10.1002/2014JC010304

Bartolacci, D. M., & Luther, M. E. (1999). Patterns of co-variability between physical and biological parameters in the Arabian Sea. *Deep-Sea Research II*, *47*(8–9), 1933–1964. https://doi.org/10.1016/S0967-0645(99)00049-1

Bassinot, F. C., Beaufort, L., Vincent, E., & Labeyrie, L. (1997). Changes in the dynamics of western equatorial Atlantic surface currents and biogenic productivity at the "Mid-Pleistocene Revolution" (~930 ka). In N. J. Shackleton, W. B. Curry, C. Richter, & T. J. Bralower (Eds.), *Proceedings of the Ocean Drilling Program, Scientific Results* (Vol. 154, pp. 269–284). Ocean Drilling Program. https://doi.org/10.2973/odp.proc.sr.154.108.1997

Bassinot, F. C., Marzin, C., Braconnot, P., Marti, O., Mathien-Blard, E., Lombard, F., & Bopp, L. (2011). Holocene evolution of summer winds and marine productivity in the tropical Indian Ocean in response to insolation forcing data-model comparison. *Climate of the Past*, *7*(3), 815–829. https://doi.org/10.5194/cp-7-815-2011

Baumann, K. H., Saavedra-Pellitero, M., Böckel, B., & Ott, C. (2016). Morphometry, biogeography and ecology of *Calcidiscus* and *Umbilicosphaera* in the South Atlantic. *Revue de Micropaleontologie*, *59*(3), 239–251. https://doi.org/10.1016/j.revmic.2016.03.001

Beaufort, L., Barbarin, N., & Gally, Y. (2014). Optical measurements to determine the thickness of calcite crystals and the mass of thin carbon particles such as coccoliths. *Nature Protocols*, *9*(3), 633–642. https://doi.org/10.1038/nprot.2014.028

Beaufort, L., Lancelot, Y., Camberlin, P., Cayre, O., Vincent, E., Bassinot, F., & Labeyrie, L. (1997). Insolation cycles as a major control of Equatorial Indian Ocean primary production. *Science*, *278*(5342), 1451–1454. https://doi.org/10.1126/science.278.5342.1451

Beaufort, L., van der Kaars, S., Bassinot, F. C., & Moron, V. (2010). Past dynamics of the Australian monsoon: Precession, phase and links to the global monsoon concept. *Climate of the Past*, *6*(5), 695–706. https://doi.org/10.5194/cp-6-695-2010

Behrenfeld, M. J., & Falkowski, P. G. (1997). Photosynthetic rates derived from satellite-based chlorophyll concentration. *Limnology and Oceanography*, *42*, 1–20. https://doi.org/10.4319/lo.1997.42.1.0001

Bialik, O. M., Auer, G., Ogawa, N. O., Kroon, D., Waldmann, N. D., & Ohkouchi, N. (2020). Monsoon, upwelling, and the deoxygenation of the northwestern Indian Ocean in response to Middle to Late Miocene global climatic shifts. *Paleoceanography and Paleoclimatology*, *35*(2), e2019PA003762. https://doi.org/10.1029/2019PA003762

Blaga, C., Reichar, G.-J., Lotter, A. F., Anselmetti, F. S., & Damsté, J. S. S. (2013). A TEX_{86} lake record suggests simultaneous shifts in temperature in Central Europe and Greenland during the last deglaciation. *Geophysical Research Letters*, *40*(5), 948–953. https://doi.org/10.1002/grl.50181

Boeckel, B., Baumann, K.-H., Henrich, R., & Kinkel, H. (2006). Coccolith distribution patterns in South Atlantic and Southern Ocean surface sediments in relation to environmental gradients. *Deep-Sea Research I*, *53*(6), 1073–1099. https://doi.org/10.1016/j.dsr.2005.11.006

Böll, A., Schulz, H., Munz, P., Rixen, T., Gaye, B., & Emeis, K.-C. (2015). Contrasting sea-surface temperature of summer and winter monsoon variability in the northern Arabian Sea over the last 25 ka. *Palaeogeography, Palaeoclimatology, Palaeoecology*, *426*, 10–21. https://doi.org/10.1016/j.palaeo.2015.02.036

Braconnot, P., Denvil, S., Foujols, M. A., Caubel, A., Marti, O., Dufresne, J.-L., et al., (2016). IPSL-CM5A-LR model output prepared for CMIP5 Mid-Holocene experiment, served by ESGF [Dataset]. World Data Center for Climate (WDCC) at DKRZ. https://doi.org/10.1594/WDCC/CMIP5.IPILmh

Braconnot, P., Harrison, S. P., Kageyama, M., Bartlein, P. J., Masson-Delmotte, V., Abe-Ouchi, A., et al. (2012). Evaluation of climate models using palaeoclimatic data. *Nature Climate Change*, *2*(6), 417–424. https://doi.org/10.1038/nclimate1456

Braconnot, P., Otto-Bliesner, B., Harrison, S., Joussaume, S., Peterchmitt, J.-Y., Abe-Ouchi, A., et al. (2007). Results of PMIP2 coupled simulations of the Mid-Holocene and Last Glacial Maximum–Part 2: Feedbacks with emphasis on the location of the ITCZ and mid- and high latitudes heat budget. *Climate of the Past*, *3*(2), 279–296. https://doi.org/10.5194/cp-3-279-2007

Broerse, A. T. C., Brummer, G.-J. A., & Van Hinte, J. E. (2000). Coccolithophores export production in response to monsoonal upwelling off Somali (northwestern Indian Ocean). *Deep-Sea Research II*, *47*, 2179–2205. https://doi.org/10.1016/S0967-0645(00)00021-7

Budziak, D., Schneider, R. R., Rostek, F., Müller, P. J., Bard, E., & Wefer, G. (2000). Late Quaternary insolation forcing on total organic carbon and C_{37} alkenone variations in the Arabian Sea. *Paleoceanography*, *15*(3), 307–321. https://doi.org/10.1029/1999PA000433

Caley, T., Zaragosi, S., Bourget, J., Martinez, P., Malaizé, B., Eynaud, F., et al. (2013). Southern Hemisphere imprint for Indo-Asian summer monsoons during the last glacial period as revealed by Arabian Sea productivity records. *Biogeosciences*, *10*(11), 7347–7359. https://doi.org/10.5194/bg-10-7347-2013

Caubel, A., Denvil, S., Foujols, M. A., Marti, O., Dufresne, J.-L., Bopp, L., et al. (2016). IPSL-CM5A-LR model output prepared for CMIP5 piControl experiment, served by ESGF [Dataset]. World Data Center for Climate (WDCC) at DKRZ. https://doi.org/10.1594/WDCC/CMIP5.IPILpc

Chang, C. P., Wang, Z., & Hendon, H. (2006). The Asian winter monsoon. In B. Wang (Ed.), *The Asian Monsoon*. Springer Berlin Geidelberg. https://doi.org/10.1007/3-540-37722-0_3

Cheng, H., Edwards, R. L., Sinha, A., Spötl, C., Yi, L., Chen, S., et al. (2016). The Asian monsoon over the past 640,000 years and ice age terminations. *Nature*, *534*(7609), 640–646. https://doi.org/10.1038/nature18591

Clark, P. U., Shakun, J. D., Baker, P. A., Bartlein, P. J., Brewer, S., Brook, E., et al. (2012). Global climate evolution during the last deglaciation. *Proceedings of the National Academy of Sciences*, *109*(19), E1134–E1142. https://doi.org/10.1073/pnas.1116619109

Collins, W. D., Bitz, C. M., Blackmon, M. L., Bonan, G. B., Bretheton, C. S., Carton, J. A., et al. (2006). The Community Climate System Model Version 3 (CCSM3). *Journal of Climate*, *19*(11), 2122–2143. https://doi.org/10.1175/JCLI3761.1

Conan, S. M.-H., & Brummer, G.-J. A. (2000). Fluxes of planktic foraminifera in response to monsoonal upwelling on the Somalia Basin margin. *Deep-Sea Research II*, *47*(9–11), 2207–2227. https://doi.org/10.1016/S0967-0645(00)00022-9

Cullen, J. L., & Prell, W. L. (1984). Planktonic foraminifera of the northern Indian Ocean: Distribution and preservation in surface sediments. *Marine Micropaleontology*, *9*, 1–52. https://doi.org/10.1016/0377-8398(84)90022-7

Curry, W. B., Ostermann, D. R., Guptha, M. V. S., & Ittekkot, V. (1992). Foraminiferal production and monsoonal upwelling in the Arabian Sea: Evidence from sediment traps. In C. P. Prell & K. C. Emeis (Eds.), *Upwelling systems: Evolution since the early Miocene* (Vol. 64, pp. 93–106). Geological Society Special Publication. https://doi.org/10.1144/GSL.SP.1992.064.01.06

Davies, C. P. (2006). Holocene paleoclimates of southern Arabian from lacustrine deposits of the Dhamar highlights, Yemen. *Quaternary Research*, *66*(3), 454–464. https://doi.org/10.1016/j.yqres.2006.05.007

de Garidel-Thoron, T., Beaufort, L., Linsley, B. K., & Dannenmann, S. (2001). Millennial-scale dynamics of the East Asian winter monsoon during the last 200,000 years. *Paleoceanography*, *16*(5), 491–502. https://doi.org/10.1029/2000PA000557

Deplazes, G., Lückge, A., Stuut, J.-B. W., Pätzold, J., Kuhlmann, H., Husson, D., et al. (2014). Weakening and strengthening of the Indian monsoon during Heinrich events and Dansgaard-Oeschger oscillations. *Paleoceanography*, *29*(2), 99–114. https://doi.org/10.1002/2013PA002509

Duchamp-Alphonse, S., Siani, G., Michel, E., Beaufort, L., Gally, Y., & Jaccard, S. L. (2018). Enhanced ocean-atmosphere carbon partitioning via the carbonate counter pump during the last deglacial. *Nature Communications*, *9*(1), 2396. https://doi.org/10.1038/s41467-018-04625-7

Dufresne, J.-L., Foujols, M.-A., Denvil, S., Caubel, A., Marti, O., Aumont, O., et al. (2013). Climate change projections using the IPSL-CM5 Earth System Model: From CMIP3 to CMIP5. *Climate Dynamics*, *40*(9–10), 2123–2165. https://doi.org/10.1007/s00382-012-1636-1

Dutt, S., Gupta, A. K., Clemens, S. C., Cheng, H., Singh, R. K., Kathayat, G., & Edwards, R. L. (2015). Abrupt changes in Indian summer monsoon strength during 33,800 to 5500 years B.P. *Gephysical Research Letters*, *42*(13), 5526–5532. https://doi.org/10.1002/2015GL064015

Emeis, K.-C., Anderson, D. M., Doose, H., Kroon, D., & Schulz-Bull, D. (1995). Sea-surface temperature and history of monsoon upwelling in the northwest Arabian Sea during the last 500,000 years. *Quaternary Research*, *43*(3), 355–361. https://doi.org/10.1006/qres.1995.1041

Engel, M., Brückner, H., Pint, A., Wellbrock, K., Ginau, A., Voss, P., et al. (2012). The early Holocene humid period in NW Saudi Arabia – Sediments, microfossils and palaeo-hydrological modelling. *Quaternary International*, *266*, 131–141. https://doi.org/10.1016/j.quaint.2011.04.028

Fincham, M., & Winter, A. (1989). Paleoceanographic interpretations of coccoliths and oxygen-isotope from the sediment surface of the southwest Indian Ocean. *Marine Micropaleontology*, *13*(4), 325–351. https://doi.org/10.1016/0377-8398(89)90024-8

Francis, D., Chaboureau, J.-P., Nelli, N., Cuesta, J., Alshamsi, N., Temimi, M., et al. (2021). Summertime dust storms over the Arabian Peninsula and impacts on radiation, circulation, cloud development and rain. *Atmospheric Research*, *250*, 105364. https://doi.org/10.1016/j.atmosres.2020.105364

Giraudeau, J. (1992). Distribution of recent nannofossil beneath the Benguela system: Southwest African continental margin. *Marine Geology*, *108*(2), 219–237. https://doi.org/10.1016/0025-3227(92)90174-G

Giraudeau, J., & Rogers, J. (1994). Phytoplankton biomass and sea-surface temperature estimates from sea-bed distribution of nannofossils and planktonic foraminifera in the Benguela upwelling system. *Micropaleontology*, *40*(3), 1825–1852. https://doi.org/10.2307/1485822

Goes, J. I., Tian, H., Gomes, H. d. R., Anderson, O. R., Al-Hashmi, K., de Rada, S., et al. (2020). Ecosystem state change in the Arabian Sea fuelled by the recent loss of snow over the Himalayan-Tibetan Plateau region. *Scientific Reports*, *10*(1), 7422. https://doi.org/10.1038/s41598-020-64360-2

25724525, 2022, 10, Downloaded from https://agupubs.onlinelibrary.wiley.com/doi/10.1029/2022PA004453 by Cochrane France, Wiley Online Library on [27/11/2022]. See the Terms and Conditions (https://onlinelibrary.wiley.com/terms-and-conditions) on Wiley Online Library for rules of use; OA articles are governed by the applicable Creative Commons License

Gravalosa, J. M., Flores, J.-A., Sierro, F. J., & Gersonde, R. (2008). Sea surface distribution of coccolithophores in the eastern Pacific sector of the Southern Ocean (Bellingshausen and Amundsen Seas) during the last austral summer of 2001. *Marine Micropaleontology*, *69*(1), 16–25. https://doi.org/10.1016/j.marmicro.2007.11.006

Guieu, C., Al Azhar, M., Aumont, O., Mahowald, N., Levy, M., Ethé, C., & Lachkar, Z. (2019). Major impact of dust deposition on the productivity of the Arabian Sea. *Geophysical Research Letters*, *46*(12), 6736–6744. https://doi.org/10.1029/2019GL082770

Gupta, A. K., Anderson, D. M., & Overpeck, J. T. (2003). Abrupt changes in the Asian southwest monsoon during the Holocene and their links to the North Atlantic Ocean. *Nature*, *421*(6921), 354–357. https://doi.org/10.1038/nature01340

Gupta, A. K., Mohan, K., Das, M., & Singh, R. K. (2013). Solar forcing Indian summer monsoon variability during the Allerød period. *Scientific Reports*, *3*(1), 2753. https://doi.org/10.1038/srep02753

Hernández-Almeida, I., Ausín, B., Saavedra-Pellitero, M., Baumann, K.-H., & Stoll, H. M. (2019). Quantitative reconstruction of primary productivity in low latitudes during the last glacial maximum and the mid-to-late Holocene from a global *Florisphaera profunda* calibration dataset. *Quaternary Science Reviews*, *205*, 166–181. https://doi.org/10.1016/j.quascirev.2018.12.016

Hersbach, H., Bell, B., Berrisford, P., Hirahara, S., Horányi, A., Muñoz-Sabater, J., et al. (2020). The ERA5 global reanalysis. *Quarterly Journal of the Royal Meteorological Society*, *146*(730), 1999–2049. https://doi.org/10.1002/qj.3803

Hoelzmann, P., Jolly, D., Harrison, S. P., Laarif, F., Bonnefille, R., & Pachur, H.-J. (1998). Mid-Holocene land-surface conditions in northern Africa and the Arabian Peninsula: A dataset for the analysis of biogeophysical feedbacks in the climate system. *Global Biogeochemical Cycles*, *12*(1), 35–51. https://doi.org/10.1029/97GB02733

Hourdin, F., Foujols, M.-A., Codron, F., Guemas, V., Dufresne, J.-L., Bony, S., et al. (2013). Impact of the LMDZ atmospheric grid configuration on the climate and sensitivity of the IPSL-CM5A coupled model. *Climate Dynamics*, *40*(9–10), 2167–2192. https://doi.org/10.1007/s00382-012-1411-3

Ivanochko, T. S., Ganeshram, R. S., Brummer, G.-J. A., Ganssen, G., Jung, S. J. A., Moreton, S. G., & Kroon, D. (2005). Variations in tropical convection as an amplifier of global climate change at the millennial scale. *Earth and Planetary Science Letters*, *235*(1–2), 302–314. https://doi.org/10.1016/j.epsl.2005.04.002

Jiang, D., Tian, Z., Lang, X., Kageyama, M., & Ramstein, G. (2015). The concept of global monsoon applied to the last glacial maximum: A multi-model analysis. *Quaternary Science Reviews*, *126*, 126–139. https://doi.org/10.1016/j.quascirev.2015.08.033

Jickells, T. D., An, Z. S., Andersen, K. K., Baler, A. R., Bergametti, G., Brooks, N., et al. (2005). Global iron connections between desert dust, ocean biogeochemistry, and climate. *Science*, *308*(5718), 67–71. https://doi.org/10.1126/science.1105959

Jiménez-Espejo, F. J., García-Alix, A., Jiménez-Moreno, G., Rodrigo-Gámiz, M., Anderson, R. S., Rodríguez-Tovar, F. J., et al. (2014). Saharan aeolian input and effective humidity variations over western Europe during the Holocene from a high altitude record. *Chemical Geology*, *374–375*, 1–12. https://doi.org/10.1016/j.chemgeo.2014.03.001

Joos, F., & Spahni, R. (2008). Rates of change in natural and anthropogenic radiative forcing over the past 20,000 years. *Proceedings of the National Academy of Sciences of the United States of America*, *105*(5), 1425–1430. https://doi.org/10.1073/pnas.0707386105

Kageyama, M., Braconnot, P., Bopp, L., Caubel, A., Foujols, M.-A., Guilyardi, E., et al. (2013). Mid-Holocene and Last Glacial Maximum climate simulations with the IPSL model. Part I: Comparing IPSL_CM5A to IPSL_CM4. *Climate Dynamics*, *40*(9–10), 2447–2468. https://doi.org/10.1007/s00382-012-1488-8

Kageyama, M., Denvil, S., Foujols, M. A., Caubel, A., Marti, O., Dufresne, J.-L., et al. (2016). IPSL-CM5A-LR model output prepared for CMIP5 lgm experiment, served by ESGF [Dataset]. World Data Center for Climate (WDCC) at DKRZ. https://doi.org/10.1594/WDCC/CMIP5.IPILlg

Kageyama, M., Merkel, U., Otto-Bliesner, B., Prange, M., Abe-Ouchi, A., Lohmann, G., et al. (2013). Climatic impacts of fresh water hosing under Last Glacial Maximum conditions: A multi-model study. *Climate of the Past*, *9*(2), 935–953. https://doi.org/10.5194/cp-9-935-2013

Kathayat, G., Cheng, H., Sinha, A., Spötl, C., Edwards, R. L., Zhang, H., et al. (2000). Indian monsoon variability on millennial-orbital timescales. *Scientific Reports*, *6*(1), 24374. https://doi.org/10.1038/srep24374

Krinner, G., Viovy, N., de Noblet-Ducoudré, N., Ogée, J., Polcher, J., Friedlingstein, P., et al. (2005). A dynamic global vegetation model for studies of the coupled atmosphere-biosphere system. *Global Biogeochemical Cycles*, *19*(1), GB1015. https://doi.org/10.1029/2003GB002199

Kudrass, H. R., Hofmann, A., Doose, H., Emeis, K., & Erlenkeuser, H. (2001). Modulation and amplification of climatic changes in the Northern Hemisphere by the Indian summer monsoon during the past 80 k.y. *Geology*, *29*(1), 63–66. https://doi.org/10.1130/0091-7613(2001)029<0063:MAAOCC>2.0.CO;2

Kumar, A., Suresh, K., & Rahaman, W. (2020). Geochemical characterization of modern aeolian dust over the Northeastern Arabian Sea: Implication for dust transport in the Arabian Sea. *Science of the Total Environment*, *729*, 138576. https://doi.org/10.1016/j.scitotenv.2020.138576

Kuper, R., & Kröpelin, S. (2006). Climate-controlled Holocene occupation in the Sahara: Motor of Africa's evolution. *Science*, *313*(5788), 803–807. https://doi.org/10.1126/science.1130989

Lambert, F., Kug, J.-S., Park, R. J., Mahowald, N., Winckler, G., Abe-Ouchi, A., et al. (2013). The role of mineral-dust aerosols in polar temperature amplification. *Nature Climate Change*, *3*(5), 487–491. https://doi.org/10.1038/nclimate1785

Lamy, F., Gersonde, R., Winckler, G., Esper, O., Jaeschke, A., Kuhn, G., et al. (2014). Increased dust deposition in the Pacific Southern Ocean during glacial periods. *Science*, *343*(6169), 403–407. https://doi.org/10.1126/science.1245424

Laskar, J., Robutel, P., Joutel, F., Gastineau, M., Correia, A. C. M., & Levrard, B. (2004). A long-term numerical solution for the insolation quantities of the Earth. *Astronomy and Astrophysics*, *428*(1), 261–285. https://doi.org/10.1051/0004-6361:20041335

Lee, C. M., Jones, B. H., Brink, K. H., & Fischer, A. S. (2000). The upper-ocean response to monsoonal forcing in the Arabian Sea: Seasonal and spatial variability. *Deep-Sea Research II*, *47*(7–8), 1177–1226. https://doi.org/10.1016/S0967-0645(99)00141-1

Le Mézo, P., Beaufort, L., Bopp, L., Braconnot, P., & Kageyama, M. (2017). From monsoon to marine productivity in the Arabian Sea: Insights from glacial and interglacial climates. *Climate of the Past*, *13*(7), 759–778. https://doi.org/10.5194/cp-13-759-2017

Lévy, M., Shankar, D., André, J.-M., Shenoi, S. S. C., Durand, F., & de Boyer Montégut, C. (2007). Basin-wide seasonal evolution of the Indian Ocean's phytoplankton blooms. *Journal of Geophysical Research*, *112*(C12), C12014. https://doi.org/10.1029/2007JC004090

Liu, C., Wang, P., Tian, J., & Cheng, X. (2008). Coccolith evidence for Quaternary nutricline variations in the southern South China Sea. *Marine Micropaleontology*, *69*(1), 42–51. https://doi.org/10.1016/j.marmicro.2007.11.008

Liu, Y., Lu, M., Yang, H., Duan, A., He, B., Yang, S., & Wu, G. (2020). Land-atmosphere-ocean coupling associated with the Tibetan Plateau and its climate impacts. *National Science Review*, *7*(3), 534–553. https://doi.org/10.1093/nsr/nwaa011

Liu, Z., Otto-Bliesner, B. L., He, F., Brady, W. C., Tomas, R., Clark, P. U., et al. (2009). Transient simulation of last deglaciation with a new mechanism for Bølling-Allerød warming. *Science*, *325*(5938), 310–314. https://doi.org/10.1126/science.1171041

Lückge, A., Ercegovac, M., Strauss, H., & Littke, R. (1999). Early diagenetic alteration of organic matter by sulfate reduction in Quaternary sediments from the northeastern Arabian Sea. *Marine Geology*, *158*(1–4), 1–13. https://doi.org/10.1016/S0025-3227(98)00191-1

Madec, G. (2008). *NEMO ocean engine, Note du pôle de modélisation*. Institut Pierre-Simon Laplace (IPSL).

25724525, 2022, 10, Downloaded from https://agupubs.onlinelibrary.wiley.com/doi/10.1029/2022PA004453 by Cochrane France, Wiley Online Library on [27/11/2022]. See the Terms and Conditions (https://onlinelibrary.wiley.com/terms-and-conditions) on Wiley Online Library for rules of use; OA articles are governed by the applicable Creative Commons License

Madhupratap, M., Prasanna Kumar, S., Bhattathiri, P. M. A., Dileep Kummar, M., Raghukumar, S., Nair, K. K. C., & Ramaiah, N. (1996). Mechanism of the biological response to winter cooling in the northeastern Arabian Sea. *Nature*, *384*(6609), 549–552. https://doi.org/10.1038/384549a0

Maher, B. A., Prospero, J. M., Mackie, D., Gaiero, D., Hesse, P. P., & Balkanski, Y. (2010). Global connections between aeolian dust, climate and ocean biogeochemistry at the present day and at the last glacial maximum. *Earth-Science Reviews*, *99*(1–2), 61–97. https://doi.org/10.1016/j.earscirev.2009.12.001

Marcott, S. A., Shakun, J. D., Clark, P. U., & Mix, A. C. (2013). A reconstruction of regional and global temperature for the past 11,300 years. *Science*, *339*(6124), 1198–1201. https://doi.org/10.1126/science.12280

Martínez-García, A., Rosell-Melé, A., Geibert, W., Gersonde, R., Masqué, P., Gaspari, V., & Barbante, C. (2009). Links between iron supply, marine productivity, sea surface temperature, and CO_2 over the last 1.1 Ma. *Paleoceanography*, *24*(1), PA1207. https://doi.org/10.1029/2008PA001657

Marzin, C., Kallel, N., Kageyama, M., Duplessy, J.-C., & Braconnot, P. (2013). Glacial fluctuations of the Indian monsoon and their relationship with North Atlantic climate: New data and modelling experiments. *Climate of the Past*, *9*(5), 2135–2151. https://doi.org/10.5194/cp-9-2135-2013

Mashat, A.-W. S., Alamoudi, A. O., Awad, A. M., & Assiri, M. E. (2018). Seasonal variability and synoptic characteristics of dust cases over southwestern Saoudi Arabia. *International Journal of Climatology*, *38*(1), 105–124. https://doi.org/10.1002/joc.5164

McManus, J. F., Francois, R., Gherardi, J.-M., Keigwin, L. D., & Brown-Leger, S. (2004). Collapse and rapid resumption of Atlantic meridional circulation linked to deglacial climate changes. *Nature*, *428*(6985), 834–837. https://doi.org/10.1038/nature02494

Molfino, B., & McIntyre, A. (1990). Precessional forcing of nutricline dynamics in the Equatorial Atlantic. *Science*, *249*(4970), 766–769. https://doi.org/10.1126/science.249.4970.766

Murton, J. B., Bateman, M. D., Dallimore, S. R., Teller, J. T., & Yang, Z. (2010). Identification of Younger Dryas outburst flood path from Lake Agassiz to the Arctic Ocean. *Nature*, *464*(7289), 740–743. https://doi.org/10.1038/nature08954

Naidu, P. D., & Malmgren, B. A. (1996). A high-resolution of late Quaternary upwelling along the Oman Margin, Arabian Sea based on planktonic foraminifera. *Paleoceanography*, *11*(1), 129–140. https://doi.org/10.1029/95PA03198

Notaro, M., Yu, Y., & Kalashnikova, O. V. (2015). Regime shift in Arabian dust activity, triggered by persistent Fertile Crescent drought. *Journal of Geophysical Research: Atmospheres*, *120*(19), 10299–10249. https://doi.org/10.1002/2015JD023855

Obase, T., & Abe-Ouchi, A. (2019). Abrupt Bølling-Allerød warming simulated under gradual forcing of the last deglaciation. *Geophysical Research Letters*, *46*(20), 11397–11405. https://doi.org/10.1029/2019GL084675

Okada, H., & Honjo, S. (1973). The distribution of oceanic coccolithophorids in the Pacific. *Deep-Sea Research*, *20*(4), 355–364. https://doi.org/10.1016/0011-7471(73)90059-4

Okada, H., & Mastsuoka, M. (1996). Lower-photic nannoflora as an indicator of the late Quaternary monsoonal palaeo-record in the tropical Indian Ocean. In *Proceedings of the "ODP and the Marine Biosphere" International Conference, 1994*.

Otto-Bliesner, B. L., Brady, E. C., Clauzet, G., Tomas, R., Levis, S., & Kothavala, Z. (2006). Last glacial maximum and Holocene climate in CCSM3. *Journal of Climate*, *19*(11), 2526–2544. https://doi.org/10.1175/JCLI3748.1

Patra, P. K., Dileep Kumar, M., Mahowald, N., & Sarma, V. V. S. S. (2007). Atmospheric deposition and surface stratification as controls of contrasting chlorophyll abundance in the North Indian Ocean. *Journal of Geophysical Research*, *112*(C5), C05029. https://doi.org/10.1029/2006JC003885

Patterson, R. T., & Fishbein, E. (1984). Re-examination of the statistical methods used to determine the number of point counts needed for micropaleontological quantitative research. *Journal of Paleontology*, *63*(2), 245–248. https://doi.org/10.1017/S0022336000019272

Peltier, W. R. (2004). Global glacial isostasy and the surface of the ice-age Earth: The ICE-5G (VM2) model and grace. *Annual Review of Earth and Planetary Sciences*, *32*(1), 111–149. https://doi.org/10.1146/annurev.earth.32.082503.144359

Pourmand, A., Marcantonio, F., Bianchi, T. S., Canuel, E. A., & Waterson, E. J. (2007). A 28-ka history of sea surface temperature, primary productivity and planktonic community variability in the western Arabian Sea. *Paleoceanography*, *22*(4), PA4208. https://doi.org/10.1029/2007PA001502

Pourmand, A., Marcantonio, F., & Schulz, H. (2004). Variations in productivity and aeolian fluxes in the northeastern Arabian Sea during the past 110 ka. *Earth and Planetary Science Letters*, *221*(1–4), 39–54. https://doi.org/10.1016/S0012-821X(04)00109-8

Prasanna Kumar, S., Madhupratap, M., Dileep Kumar, M., Muraleedharan, P. M., de Souza, S. N., Ganus, M., & Sarma, V. V. S. S. (2001). High biological productivity in the central Arabian Sea during the summer monsoon driven by Ekman pumping and lateral advection. *Current Science*, *81*, 1633–1638.

Prasanna Kumar, S., Muraleedharan, P. M., Prasad, T. G., Ganus, M., Ramaiah, N., de Souza, S. N., et al. (2002). Why is the Bay of Bengal less productive during summer monsoon compared to the Arabian Sea? *Geophysical Research Letters*, *29*(24), 2235. https://doi.org/10.1029/2002GL016013

Prasanna Kumar, S., & Narvekar, J. (2005). Seasonal variability of the mixed layer in the central Arabian Sea and its implication on nutrients and primary productivity. *Deep-Sea Research II*, *52*(14–15), 1848–1861. https://doi.org/10.1016/j.dsr2.2005.06.002

Prasanna Kumar, S., Ramaiah, N., Ganus, M., Sarma, V. V. S. S., Muraleedharan, P. M., Raghukumar, S., et al. (2001). Physical forcing of biological productivity in the Northern Arabian Sea during the Northeast Monsoon. *Deep-Sea Research II*, *48*(6–7), 1115–1126. https://doi.org/10.1016/S0967-0645(00)00133-8

Ramaswamy, V., Muraleedharan, P. M., & Prakash Babu, C. (2017). Mid-troposphere transport of Middle-East dust over the Arabian Sea and its effect on rainwater composition and sensitive ecosystems over India. *Scientific Reports*, *7*(1), 13676. https://doi.org/10.1038/s41598-017-13652-1

Rea, D. K. (1994). The paleoclimatic record provided by eolian deposition in the deep sea: The geologic history of wind. *Reviews of Geophysics*, *32*(2), 159–195. https://doi.org/10.1029/93RG03257

Reichart, G.-J., Brinkhuis, H., Huiskamp, F., & Zachariasse, W. J. (2004). Hyperstratification following glacial overturning events in the northern Arabian Sea. *Paleoceanography*, *19*(2), PA2013. https://doi.org/10.1029/2003PA000900

Reichart, G. J., den Dulk, M., Visser, H. J., van der Weijden, C. H., & Zachariasse, W. J. (1997). A 225 kyr record of dust supply, paleoproductivity and the oxygen minimum zone from the Murray Ridge (northern Arabian Sea). *Palaeogeography, Palaeoclimatology, Palaeoecology*, *134*(1–4), 149–169. https://doi.org/10.1016/S0031-0182(97)00071-0

Renaud, S., Ziveri, P., & Broerse, A. T. C. (2002). Geographical and seasonal differences in morphology and dynamics of the coccolithophore *Calcidiscus leptoporus*. *Marine Micropaleontology*, *46*(3–4), 363–385. https://doi.org/10.1016/S0377-8398(02)00081-6

Renssen, H., & Isarin, R. F. B. (2001). The two major warming phases of the last deglaciation at ~14.7 and ~11.5 ka cal BP in Europe: Climate reconstructions and AGCM experiments. *Global and Planetary Change*, *30*(1–2), 117–153. https://doi.org/10.1016/S0921-8181(01)00082-0

Reynolds, R. W., Smith, T. M., Liu, C., Chelton, D. B., Casey, K. S., & Schlax, M. G. (2007). Daily high-resolution-blended analyses for sea surface temperature. *Journal of Climate*, *20*(22), 5473–5496. https://doi.org/10.1175/2007JCLI1824.1

25724525, 2022, 10, Downloaded from https://agupubs.onlinelibrary.wiley.com/doi/10.1029/2022PA004453 by Cochrane France, Wiley Online Library on [27/11/2022]. See the Terms and Conditions (https://onlinelibrary.wiley.com/terms-and-conditions) on Wiley Online Library for rules of use; OA articles are governed by the applicable Creative Commons License

Rezazadeh, M., Irannejad, P., & Shao, Y. (2013). Climatology of the Middle East dust events. *Aeolian Research*, *10*, 103–109. https://doi.org/10.1016/j.aeolia.2013.04.001

Rogalla, U., & Andruleit, H. (2005). Precessional forcing of coccolithophore assemblages in the northern Arabian Sea: Implications for monsoonal dynamics during the last 200,000 years. *Marine Geology*, *217*(1–2), 31–48. https://doi.org/10.1016/j.margeo.2005.02.028

Saavedra-Pellitero, M., Flores, J. A., Baumann, K.-H., & Sierro, F. J. (2010). Coccolith distribution patterns in surface sediments of Equatorial and Southeastern Pacific Ocean. *Geobios*, *43*(1), 131–149. https://doi.org/10.1016/j.geobios.2009.09.004

Safaierad, R., Mohtadi, M., Zolitschka, B., Yokoyama, Y., Vogt, C., & Schefuß, E. (2020). Elevated dust depositions in West Asia linked to ocean–atmosphere shifts during North Atlantic cold events. *Proceedings of the National Academy of Sciences of the United States of America*, *117*(31), 18272–18277. https://doi.org/10.1073/pnas.2004071117

Schott, F. A., & McCreary, J. P. (2001). The monsoon circulation of the Indian Ocean. *Progress in Oceanography*, *52*, 1–123. https://doi.org/10.1016/S0079-6611(01)00083-0

Schulte, S., & Müller, P. J. (2001). Variations of sea surface temperature and primary productivity during Heinrich and Dansgaard-Oeschger events in the northwestern Arabian Sea. *Geo-Marine Letters*, *21*(3), 168–175. https://doi.org/10.1007/s003670100080

Schulz, H., von Rad, U., Erlenkeuser, H., & von Rad, U. (1998). Correlation between Arabian Sea and Greenland climate oscillations of the past 110,000 years. *Nature*, *393*(6680), 54–57. https://doi.org/10.1038/31750

Shakun, J. D., Burns, S. J., Fleitmann, D., Kramers, J., Matter, A., & Al-Subary, A. (2007). A high-resolution, absolute dated deglacial speleothem record of Indian Ocean climate from Socotra Island, Yemen. *Earth and Planetary Science Letters*, *259*(3–4), 442–456. https://doi.org/10.1016/j.epsl.2007.05.004

Shakun, J. D., Clark, P. U., He, F., Marcott, S. A., Mix, A. C., Liu, Z., et al. (2012). Global warming preceded by increasing carbon dioxide concentrations during the last deglaciation. *Nature*, *484*(7392), 49–54. https://doi.org/10.1038/nature10915

Shimmield, G. B., Mowbray, S. R., & Weedon, G. P. (1990). A 350 ka history of the Indian Southwest Monsoon—Evidence from deep-sea cores, northwest Arabian Sea. *Transactions of the Royal Society of Edinburgh Earth Sciences*, *81*(4), 289–299. https://doi.org/10.1017/S0263593300020800

Singh, R. P., Prasad, A. K., Kayetha, V. K., & Kafatos, M. (2008). Enhancement of oceanic parameters associated with dust storms using satellite data. *Journal of Geophysical Research*, *113*(C11), C11008. https://doi.org/10.1029/2008JC004815

Sirocko, F., Garbe-Schönberg, D., & Devey, C. (2000). Processes controlling trace element geochemistry of Arabian Sea sediments during the last 25,000 years. *Global and Planetary Change*, *26*(1–3), 217–303. https://doi.org/10.1016/S0921-8181(00)00046-1

Sirocko, F., Sarnthein, M., Lange, H., & Erlenkeuser, H. (1991). Atmospheric summer circulation and coastal upwelling in the Arabian Sea during the Holocene and the last glaciation. *Quaternary Research*, *36*(1), 72–93. https://doi.org/10.1016/0033-5894(91)90018-Z

Sowers, T., & Bender, M. (1995). Climate records covering the last deglaciation. *Science*, *269*(5221), 210–214. https://doi.org/10.1126/science.269.5221.210

Stuiver, M., & Grootes, P. M. (2000). GISP2 oxygen isotope ratios. *Quaternary Research*, *53*(3), 277–284. https://doi.org/10.1006/qres.2000.2127

Su, X., Liu, C., Beaufort, L., Tian, J., & Huang, E. (2013). Late Quaternary coccolith records in the South China Sea and East Asian monsoon dynamics. *Global and Planetary Change*, *111*, 88–96. https://doi.org/10.1016/j.gloplacha.2013.08.016

Swann, A. L. S., Fung, I. Y., Liu, Y., & Chiang, J. C. H. (2014). Remote vegetation feedbacks and the Mid-Holocene Green Sahara. *Journal of Climate*, *27*(13), 4857–4870. https://doi.org/10.1175/JCLI-D-13-00690.1

Tamburini, F., Föllmi, K. B., Adatte, T., Bernasconi, S. M., & Steinmann, P. (2003). Sedimentary phosphorus record from the Oman margin: New evidence of high productivity during glacial periods. *Paleoceanography*, *18*(1), 1015. https://doi.org/10.1029/2000PA000616

Taylor, K. E., Stouffer, R. J., & Meehl, G. A. (2012). An overview of CMIP5 and the experiment design. *Bulletin of the American Meteorological Society*, *93*(4), 485–498. https://doi.org/10.1175/BAMS-D-11-00094.1

Tian, Z., & Jiang, D. (2016). Revisiting last glacial maximum climate over China and East Asian monsoon using PMIP3 simulations. *Palaeogeography, Palaeoclimatology, Palaeoecology*, *453*, 115–126. https://doi.org/10.1016/j.palaeo.2016.04.020

Tierney, J. E., Russel, J. M., Huang, Y., Damsté, J. S. S., Hapmans, E. C., & Cohen, A. S. (2008). Northern Hemisphere controls on tropical southeast African climate during the past 60,000 years. *Science*, *322*(5899), 252–255. https://doi.org/10.1126/science.1160485

Tierney, J. E., Zhu, J., King, J., Malevich, S. B., Hakim, G. J., & Poulsen, C. J. (2020). Glacial cooling and climate sensitivity revisited. *Nature*, *584*(7822), 569–573. https://doi.org/10.1038/s41586-020-2617-x

Wang, B., & Ding, Q. (2008). Global monsoon: Dominant mode of annual variation in the tropics. *Dynamics of Atmospheric and Oceans*, *44*(3–4), 165–183. https://doi.org/10.1016/j.dynatmoce.2007.05.002

Weedon, G. P., & Shimmield, G. B. (1991). Late Pleistocene upwelling and productivity variations in the northwest Indian Ocean deduced from spectral analyses of geochemical data from sites 722 and 724. In W. L. Prell, N. Niitsuma, K.-C. Emeis, Z. K. Al-Sulaiman, A. N. K. Al-Tobbah, D. M. Anerson, et al. (Eds.), *Proceedings of the Ocean Drilling Program, Scientific Results* (Vol. 117, pp. 431–443). Ocean Drilling Program. https://doi.org/10.2973/odp.proc.sr.117.171.1991

Wen, X., Liu, Z., Wang, S., Cheng, J., & Zhu, J. (2016). Correlation and anti-correlation of the East Asian summer and winter monsoons during the last 21,000 years. *Nature Communications*, *7*(1), 11999. https://doi.org/10.1038/ncomms11999

Winckler, G., Anderson, R. F., Fleisher, M. Q., McGee, D., & Mahowald, N. (2008). Covariant glacial-interglacial dust fluxes in the equatorial Pacific and Antarctica. *Science*, *320*(5872), 93–96. https://doi.org/10.1126/science.1150595

Yu, Y., Notaro, M., Liu, Z., Kalashnikova, O., Alkolibi, F., Fadda, E., & Bakhrjy, F. (2013). Assessing temporal and spatial variations in atmospheric dust over Saudi Arabian through satellite, radiometric, and station data. *Journal of Geophysical Research: Atmospheres*, *118*(23), 13253–13264. https://doi.org/10.1002/2013JD020677

Zhang, H., Liu, C., Jin, X., Shi, J., Zhao, S., & Jian, Z. (2016). Dynamics of primary productivity in the northern South China Sea over the past 24,000 years. *Geochemistry, Geophysics, Geosystems*, *17*(12), 4878–4891. https://doi.org/10.1002/2016GC006602

Zhou, X., Duchamp-Alphonse, S., Kageyama, M., Bassinot, F., Beaufort, L., & Colin, C. (2020). Dynamics of primary productivity in the northeastern Bay of Bengal over the last 26000 years. *Climate of the Past*, *16*(5), 1969–1986. https://doi.org/10.5194/cp-16-1969-2020

Zhou, X., Duchamp-Alphonse, S., Kageyama, M., Bassinot, F., Doressoundiram, F., & Kissel, C. (2022). Coccolith counting and reconstructed primary productivity results of core MD00-2354 [Dataset]. PANGAEA. https://doi.org/10.1594/PANGAEA.946822

Ziegler, M., Lourens, L. J., Tuenter, E., & Reichart, G.-J. (2010). High Arabian Sea productivity conditions during MIS 13 – Odd monsoon event or intensified overturning circulation at the end of Mid-Pleistocene transition? *Climate of the Past*, *6*(1), 63–76. https://doi.org/10.5194/cp-6-63-2010

Ziveri, P., Thunell, R. C., & Rio, D. (1995). Export production of coccolithophores in an upwelling region: Results from San Pedro Basin, Southern California Borderlands. *Marine Micropaleontology*, *24*(3–4), 335–358. https://doi.org/10.1016/0377-8398(94)00017-H

25724525, 2022, 10, Downloaded from https://agupubs.onlinelibrary.wiley.com/doi/10.1029/2022PA004453 by Cochrane France, Wiley Online Library on [27/11/2022]. See the Terms and Conditions (https://onlinelibrary.wiley.com/terms-and-conditions) on Wiley Online Library for rules of use; OA articles are governed by the applicable Creative Commons License